Supplemental Information

The clinical drug candidate anle138b binds predominantly to the central cavity in lipidic $A\beta_{40}$ fibrils and modulates fibril formation.

Mookyoung Han[1], Benedikt Frieg[2], Dirk Matthes[3], Andrei Leonov[1,4], Sergey Ryazanov[1,4], Karin Giller[1], Evgeny Nimerovsky[1], Marianna Stampolaki[1], Kai Xue[1], Kerstin Overkamp[1], Christian Dienemann[5], Dietmar Riedel[6], Armin Giese[4], Stefan Becker[1], Bert L. de Groot[3], Gunnar F. Schröder[2,7], Loren B. Andreas[1*] and Christian Griesinger[1,8*]

[1.] Department of NMR-Based Structural Biology, Max Planck Institute for Multidisciplinary Sciences; Göttingen, Germany.

[2.] Ernst-Ruska Centre for Microscopy and Spectroscopy with Electrons, ER-C-3 Structural Biology, Forschungszentrum Jülich, Jülich, Germany

[3.] Department of Theoretical and Computational Biophysics, Max Planck Institute for Multidisciplinary Sciences; Göttingen, Germany.

[4.] MODAG GmbH, Mikroforum Ring 3, 55234, Wendelsheim, Germany

[5.] Department of Molecular Biology, Max Planck Institute for Multidisciplinary Sciences; Göttingen, Germany.

[6.] Laboratory of Electron Microscopy, Max-Planck-Institute for Multidisciplinary Sciences, Göttingen, Germany.

[7.] Physics Department, Heinrich Heine University Düsseldorf; Düsseldorf, Germany

[8.] Cluster of Excellence "Multiscale Bioimaging: From Molecular Machines to Networks of Excitable Cells" (MBExC), University of Göttingen; Göttingen, Germany.

* Correspondence and requests for materials should be addressed to Loren B. Andreas (land@mpinat.mpg.de) and Christian Griesinger (cigr@mpinat.mpg.de).

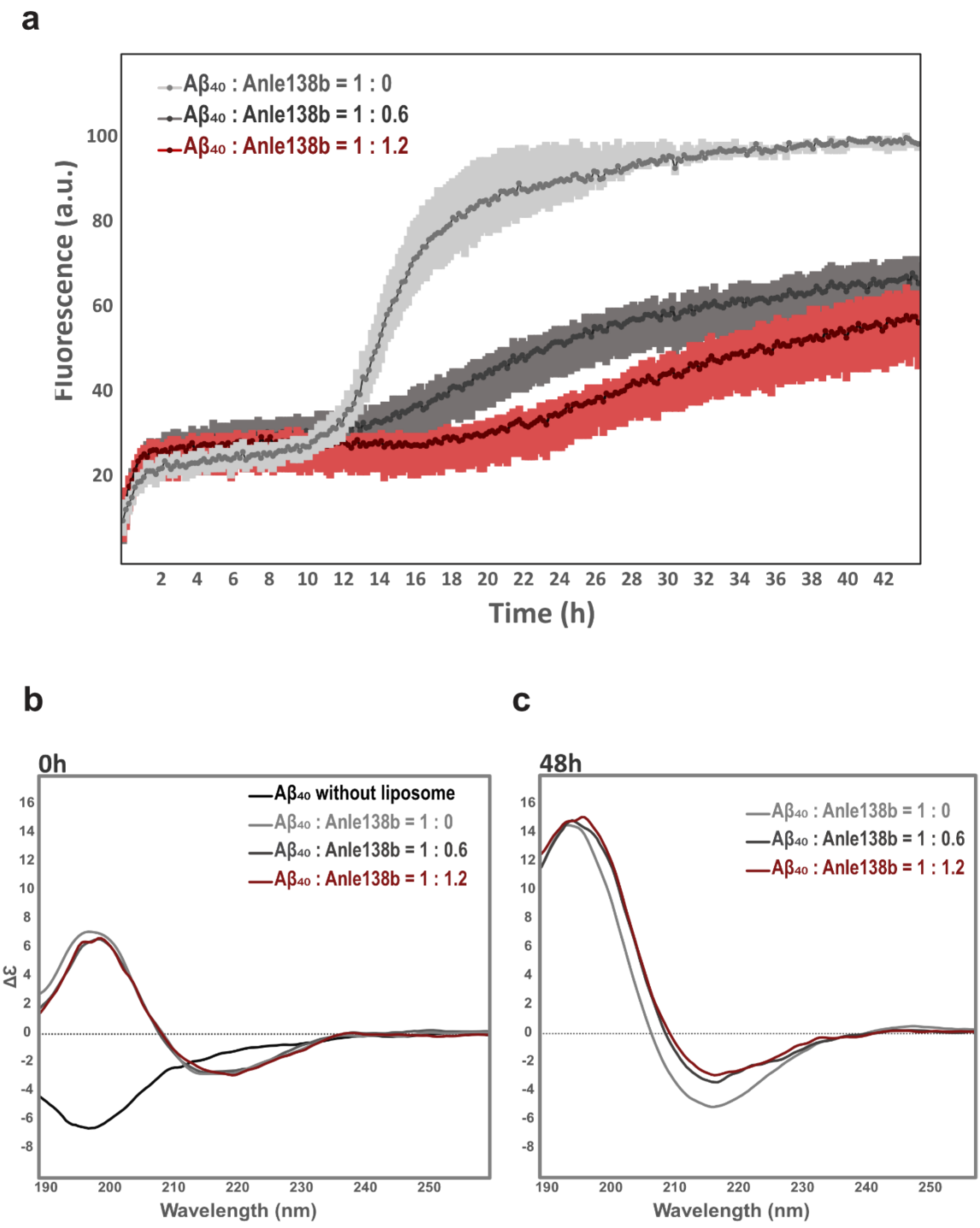
a
Aβ40 : Anle138b = 1 : 0
Aβ40 : Anle138b = 1 : 0.6
Aβ40 : Anle138b = 1 : 1.2
Fluorescence (a.u.)
Time (h)
b
0h
Aβ40 without liposome
Aβ40 : Anle138b = 1 : 0
Aβ40 : Anle138b = 1 : 0.6
Aβ40 : Anle138b = 1 : 1.2
Δε
Wavelength (nm)
c
48h
Aβ40 : Anle138b = 1 : 0
Aβ40 : Anle138b = 1 : 0.6
Aβ40 : Anle138b = 1 : 1.2
Wavelength (nm)

Supplementary Figure 1 | Anle138b modulates L1 $A\beta_{40}$ fibril formation and secondary structure under the pre-treatment condition.

a. The ThT fluorescence assay shows the effect of increasing concentrations of anle138b on $A\beta_{40}$ fibril formation. The control fibrils ($A\beta_{40}$: anle138b [SMPR] = 1:0) are shown in light gray, the intermediate concentration (SMPR = 1:0.6) in dark gray, and the high concentration (SMPR = 1:1.2) in red. At the highest concentration, anle138b extends the lag phase by approximately 8–10 hours and reduces the overall ThT fluorescence intensity by 40–60%. **b.** Circular dichroism (CD) spectra acquired at 0 hours show β-sheet formation in all conditions (SMPR = 1:0, 1:0.6, and 1:1.2; light gray, dark gray, red). No significant differences were observed between the formation of the β-sheet in the presence or absence of anle138b. **c.** CD spectra after 48 hours of incubation reveal strong β-sheet content in the control fibrils (light gray), while fibrils treated with anle138b (dark gray for SMPR = 1:0.6, red for SMPR = 1:1.2) exhibit reduced β-sheet formation.

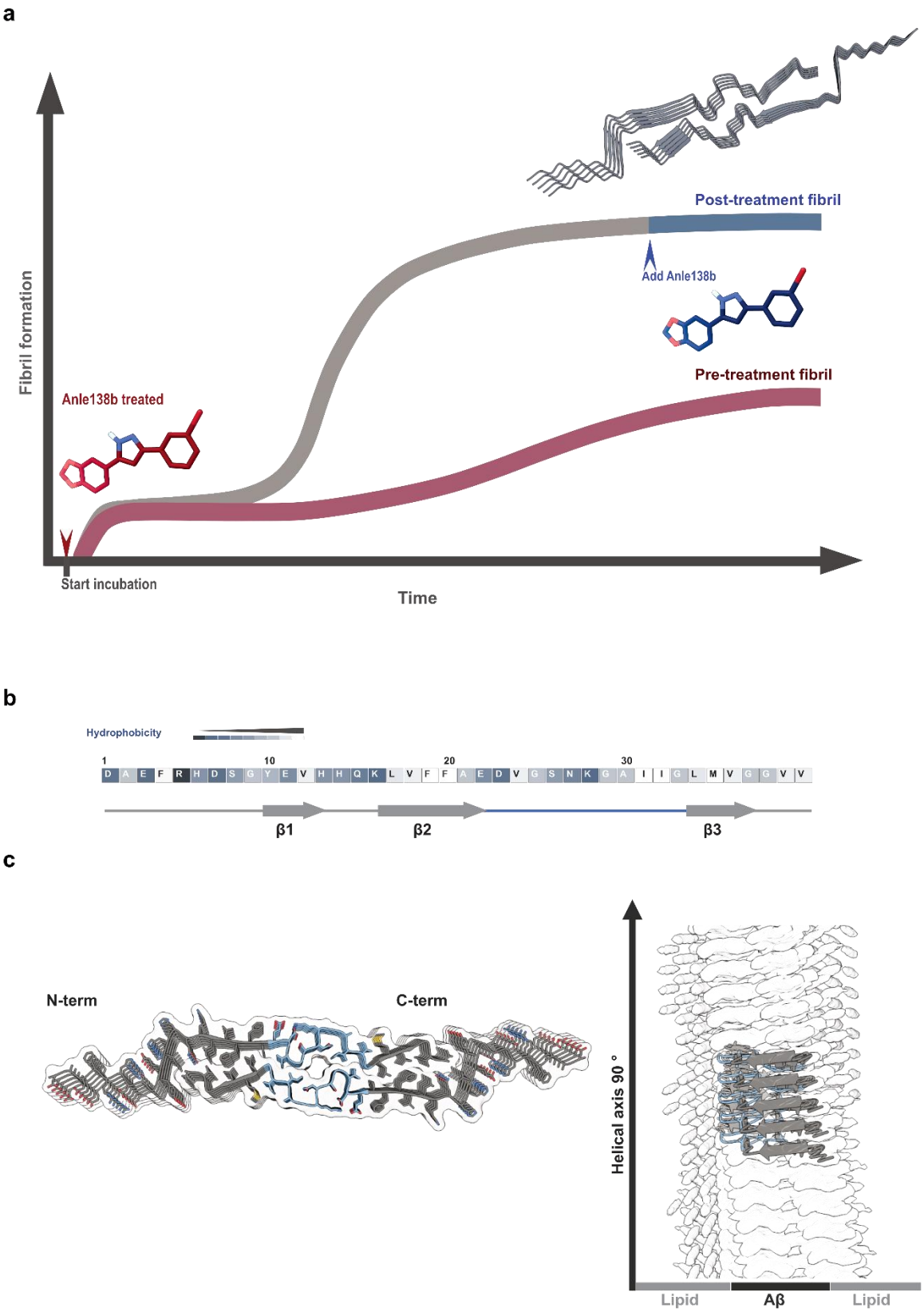
a
Post-treatment fibril
Add Anle138b
Pre-treatment fibril
Anle138b treated
Fibril formation
Start incubation
Time
b
Hydrophobicity
1
10
20
30
D A E F R H D S G Y E V H H Q K L V F F A E D V G S N K G A I I G L M V G G V V
β1
β2
β3
c
N-term
C-term
Helical axis 90 °
Lipid
Aβ
Lipid

44

45

Supplementary Figure 2 | Schematic illustration of experiments investigating the binding sites of anle138b on L1 Aβ$_{40}$ fibrils.

a. Schematic illustration of L1 Aβ$_{40}$ fibril formation under pre-treatment and post-treatment conditions. In the post-treatment condition, anle138b (blue) is added after fibril formation. In the pre-treatment condition, fibrils form in the presence of anle138b (red), which extends the lag phase and reduces the final fibril amount. The two arrows indicate the time points at which anle138b was administered during the fibril formation process. Blue represents the post-treatment condition, and red represents the pre-treatment condition. **b.** Amino acid sequence and secondary structure of the L1 Aβ$_{40}$ fibril. Hydrophobicity is color-coded using a gradient from dark blue (hydrophilic) to white (hydrophobic), based on the Eisenberg scale[65]. The loop region (Ala21–Gly33), highlighted in blue, contributes to the formation of the central cavity between the two protofilaments. **c.** Structure of the L1 Aβ$_{40}$ fibril based on cryo-EM data. Left: Top view of the fibril showing the loop region (blue). Right: Side view highlighting the periodic alignment of rod-shaped lipid densities along the fibril axis, as visualized in the cryo-EM map.

a

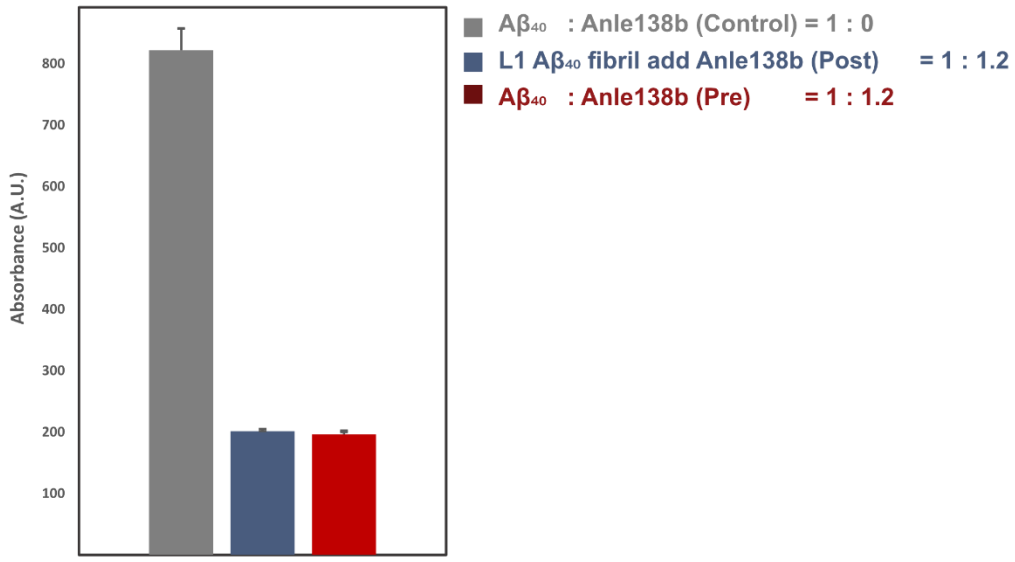
Aβ40 : Anle138b (Control) = 1 : 0
L1 Aβ40 fibril add Anle138b (Post) = 1 : 1.2
Aβ40 : Anle138b (Pre) = 1 : 1.2
Absorbance (A.U.)
800
700
600
500
400
300
200
100

b

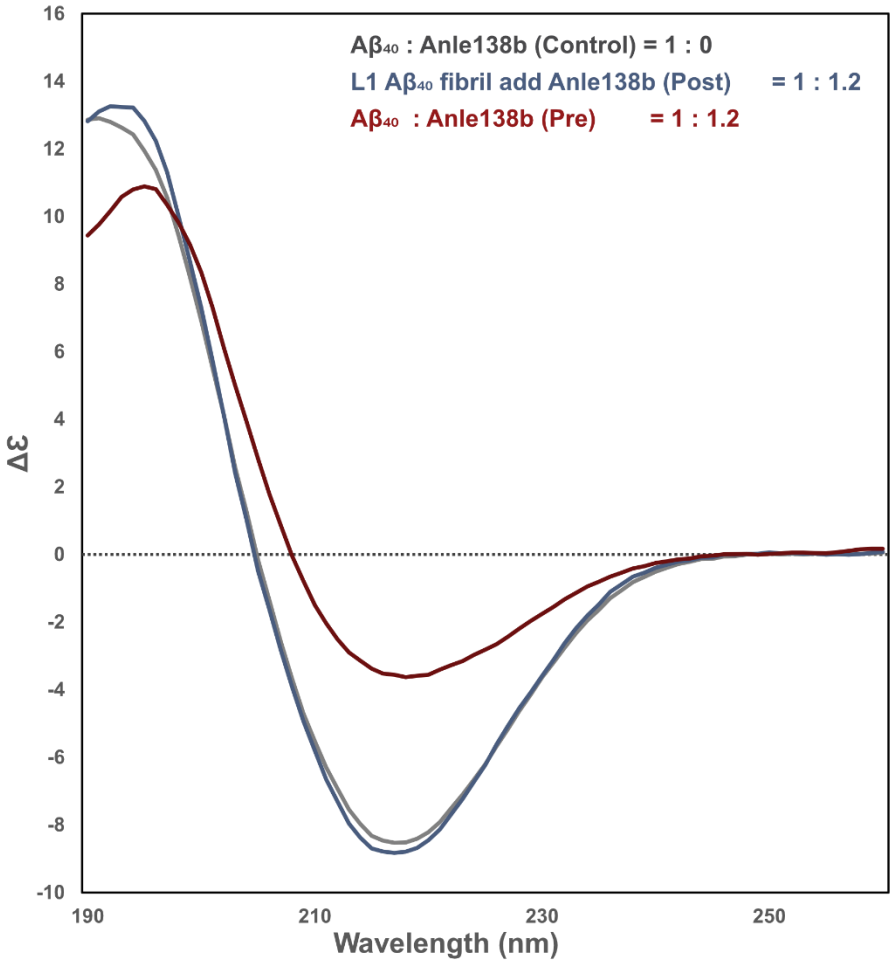
Aβ40 : Anle138b (Control) = 1 : 0
L1 Aβ40 fibril add Anle138b (Post) = 1 : 1.2
Aβ40 : Anle138b (Pre) = 1 : 1.2
Δε
16
14
12
10
8
6
4
2
0
-2
-4
-6
-8
-10
190
210
230
250
Wavelength (nm)

Supplementary Figure 3 | Effects of anle138b on L1 Aβ$_{40}$ fibril formation and structural interaction.

The results shown here were obtained from the same sample sets used for cryo-EM (Fig. 2) as well as in negative-stain EM, 1D (^{1}H) ^{15}N CP NMR experiments (Fig. 1b, c), 2D ^{13}C^{13}C-DARR spectra (Supplementary Figs. 15, 16), and 2D (H)NCA spectra (Supplementary Fig 5). **a.** ThT fluorescence assay of L1 Aβ$_{40}$ fibrils prepared under three different conditions. The control sample contains(gray) in the absence of anle138b. In the post-treatment condition (blue; SMPR = 1:1.2) and in the pre-treatment condition (red; SMPR = 1:1.2). **b.** CD spectra of L1 Aβ$_{40}$ fibrils under the same conditions as in **a**. The control (gray) shows characteristic β-sheet content. The post-treatment condition (blue) exhibits a spectrum similar to the control, indicating that the β-sheet structure is largely preserved. In contrast, the pre-treatment condition (red), where anle138b was present during fibril formation, shows less β-sheet content.

a

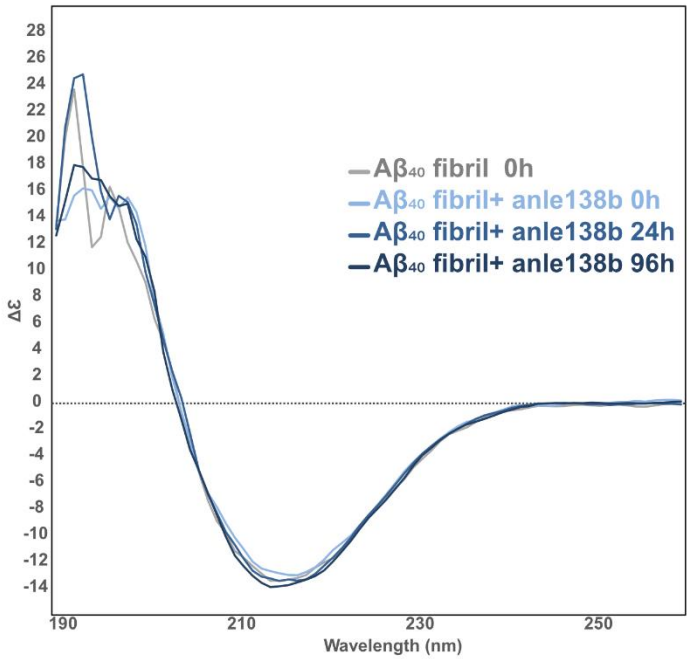
Aβ40 fibril 0h
Aβ40 fibril+ anle138b 0h
Aβ40 fibril+ anle138b 24h
Aβ40 fibril+ anle138b 96h
Δε
Wavelength (nm)
28
26
24
22
20
18
16
14
12
10
8
6
4
2
0
-2
-4
-6
-8
-10
-12
-14
190
210
230
250

b

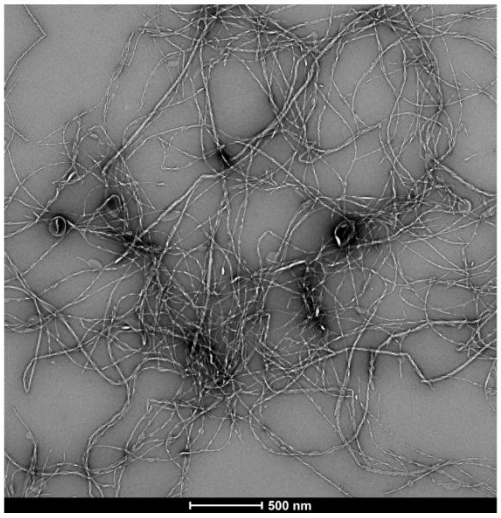
500 nm

c

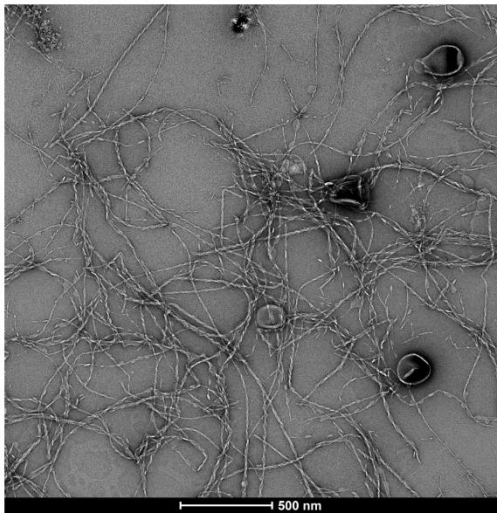
500 nm

Supplementary Figure 4 | CD spectroscopy and negative-stain EM analysis of L1 $A\beta_{40}$ fibrils under post-treatment condition (SMPR = 1:1.2).

The secondary structure of L1 $A\beta_{40}$ fibrils treated with anle138b was assessed by CD spectroscopy under post-treatment conditions, following incubation at 37 °C for up to 96 hours. **a.** CD spectra of L1 $A\beta_{40}$ fibrils at various time points after anle138b addition: untreated (gray, 0 h), immediately after treatment (light blue, 0 h), 24 h (blue), and 96 h (dark blue). **b, c.** Negative-stain EM images of L1 $A\beta_{40}$ fibrils at 0 h and 96 h after anle138b treatment.

a

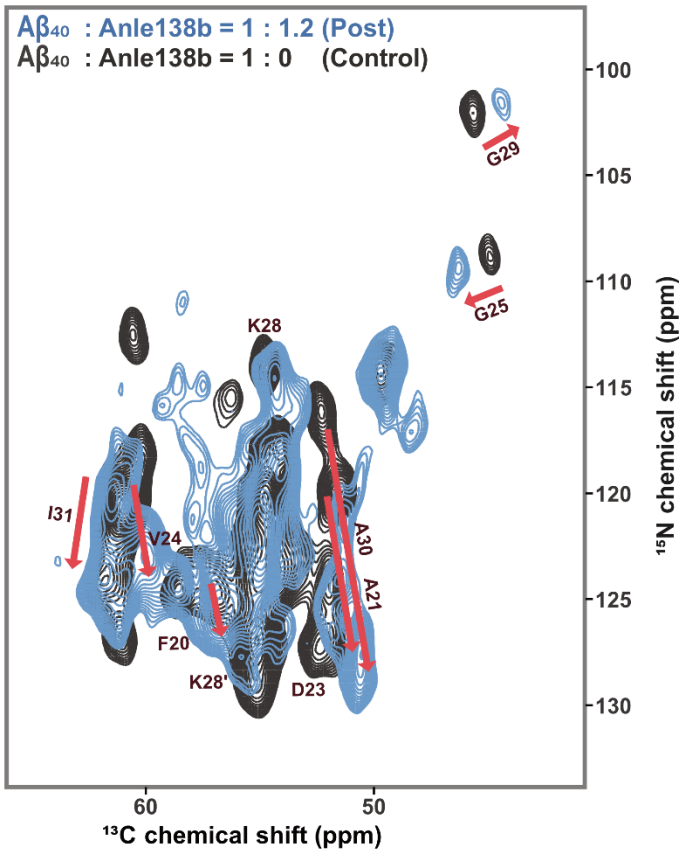
Aβ40 : Anle138b = 1 : 1.2 (Post)
Aβ40 : Anle138b = 1 : 0 (Control)
G29
G25
K28
I31
V24
F20
K28'
D23
A30
A21
100
105
110
115
120
125
130
60
50
13C chemical shift (ppm)
15N chemical shift (ppm)

b

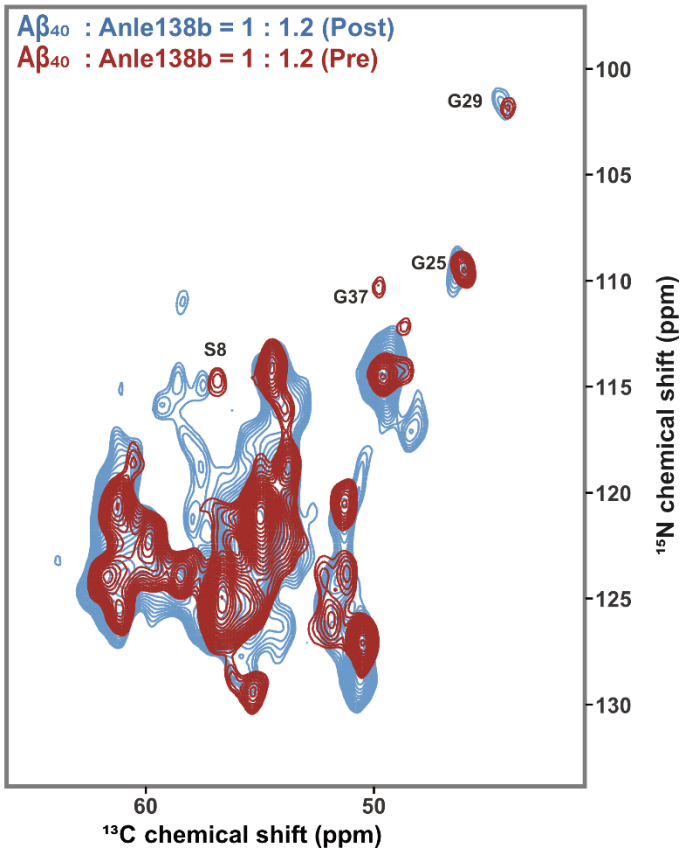
Aβ40 : Anle138b = 1 : 1.2 (Post)
Aβ40 : Anle138b = 1 : 1.2 (Pre)
G29
G25
G37
S8
100
105
110
115
120
125
130
60
50
13C chemical shift (ppm)
15N chemical shift (ppm)

Supplementary Figure 5 | Superimposed 2D (H)NCA spectra of L1 $A\beta_{40}$ fibrils under control, pre-treatment, and post-treatment conditions.

The spectra were obtained from the same sample sets utilized in cryo-EM (Fig. 2, Supplementary Figs. 6, 7), negative-stain EM, and solid-state NMR experiments (Fig. 1b, c, Supplementary Figs. 15, 16). **a.** Superimposed 2D (H)NCA spectra of L1 $A\beta_{40}$ fibrils. The blue spectrum represents fibrils treated with anle138b after fibril formation (post-treatment condition; $A\beta_{40}$: anle138b [SMPR] = 1:1.2, ns = 64), while the black spectrum corresponds to fibrils formed in the absence of anle138b (control condition; ns = 64). Chemical shift perturbations induced by anle138b treatment are indicated by pink arrows. **b.** Superimposed 2D (H)NCA spectra comparing the pre- and post-treatment conditions. The red spectrum represents fibrils formed in the presence of anle138b during aggregation (pre-treatment; SMPR = 1:1.2, ns = 192), while the blue spectrum corresponds to the post-treatment condition (SMPR = 1:1.2, ns = 64).

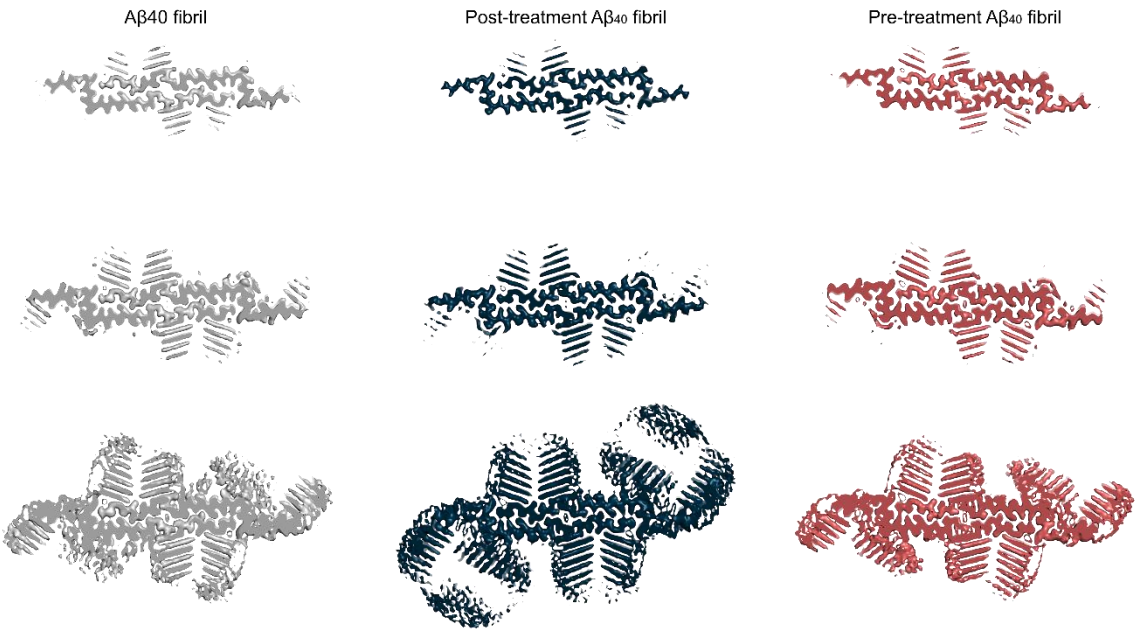

Supplementary Figure 6 | Sharpened high-resolution maps at different iso-surface levels, L1 Aβ$_{40}$ fibrils.

From the top to the bottom, the iso-surface level threshold decreases such that additional low-resolution features become visible.

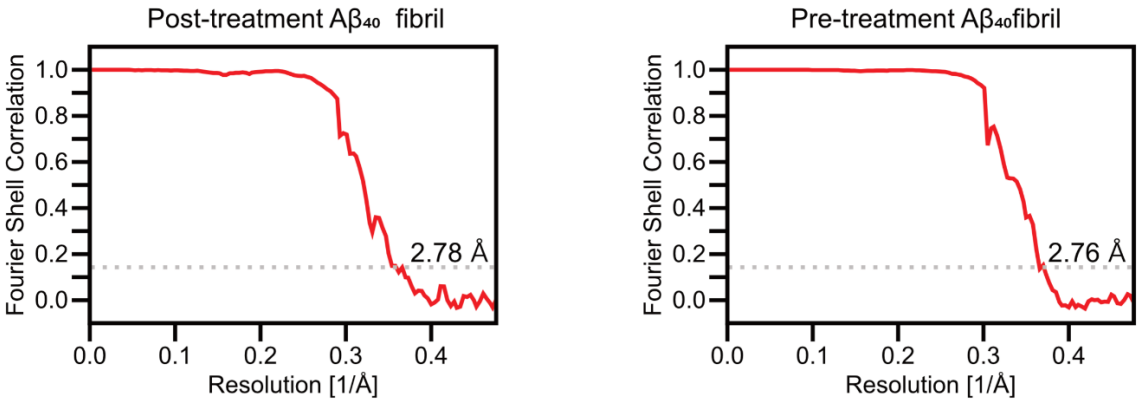

Supplementary Figure 7 | Fourier shell correlation curves.

Masked-corrected (z-percentage is 0.1) Fourier shell correlation (FSC) curves. The final resolution is shown in the plot and was estimated from the value of the FSC curve for two separately refined masked half-maps at 0.143 (red line).

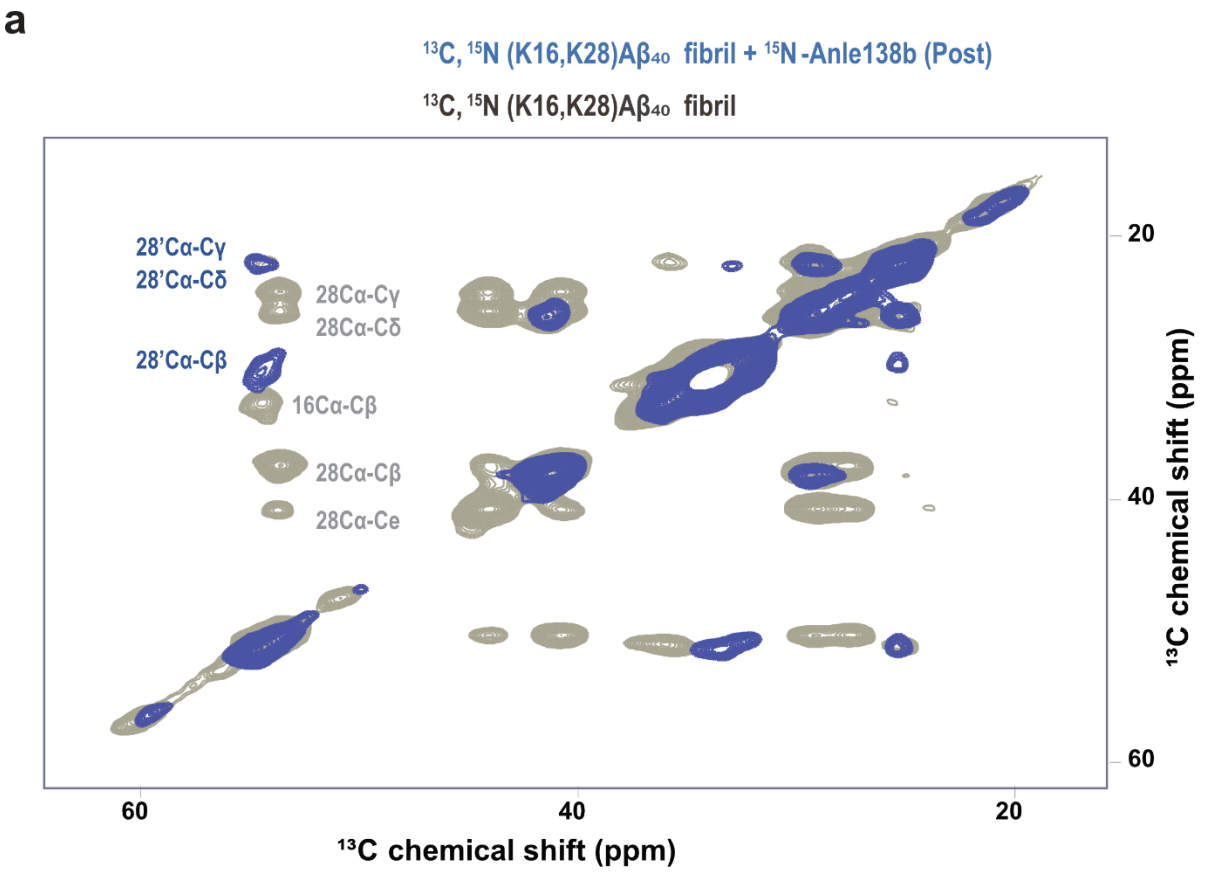
a
^{13}C, ^{15}N (K16,K28)Aβ$_{40}$ fibril + ^{15}N-Anle138b (Post)
^{13}C, ^{15}N (K16,K28)Aβ$_{40}$ fibril
28'Cα-Cγ
28'Cα-Cδ
28Cα-Cγ
28Cα-Cδ
28'Cα-Cβ
16Cα-Cβ
28Cα-Cβ
28Cα-Ce
20
40
60
^{13}C chemical shift (ppm)
60
40
20
^{13}C chemical shift (ppm)

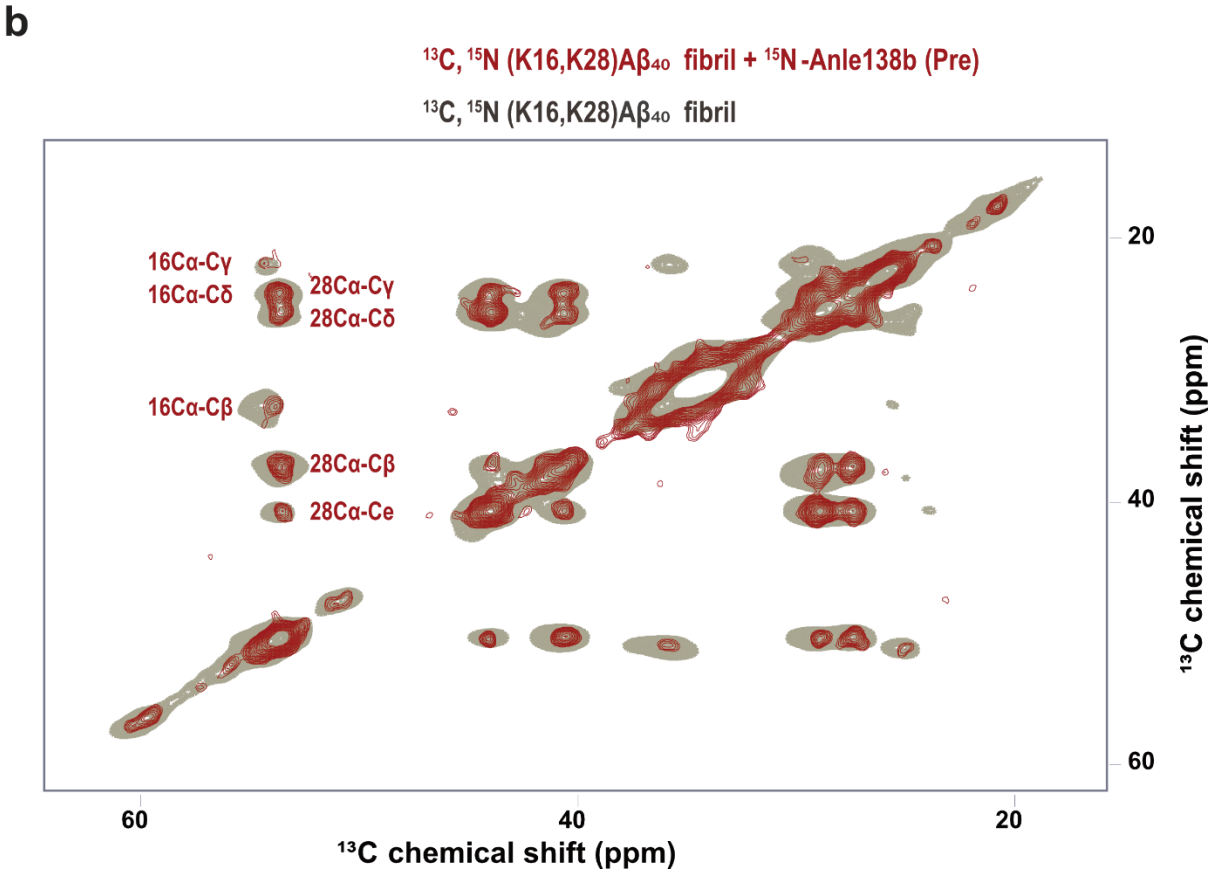
b
^{13}C, ^{15}N (K16,K28)Aβ$_{40}$ fibril + ^{15}N-Anle138b (Pre)
^{13}C, ^{15}N (K16,K28)Aβ$_{40}$ fibril
16Cα-Cγ
16Cα-Cδ
28Cα-Cγ
28Cα-Cδ
16Cα-Cβ
28Cα-Cβ
28Cα-Ce
20
40
60
^{13}C chemical shift (ppm)
60
40
20
^{13}C chemical shift (ppm)

Supplementary Figure 8 | 2D $^{13}C^{13}C$-DARR spectra of L1 Aβ$_{40}$ fibrils selectively labeled with ^{13}C, ^{15}N at Lys16 and Lys28.

a. 2D $^{13}C^{13}C$-DARR spectrum acquired at 265 K and 850 MHz with a mixing time of 20 ms. The blue spectrum corresponds to the post-treatment condition. **b.** The red spectrum represents the pre-treatment condition. In both panels, the gray spectrum represents the control condition.

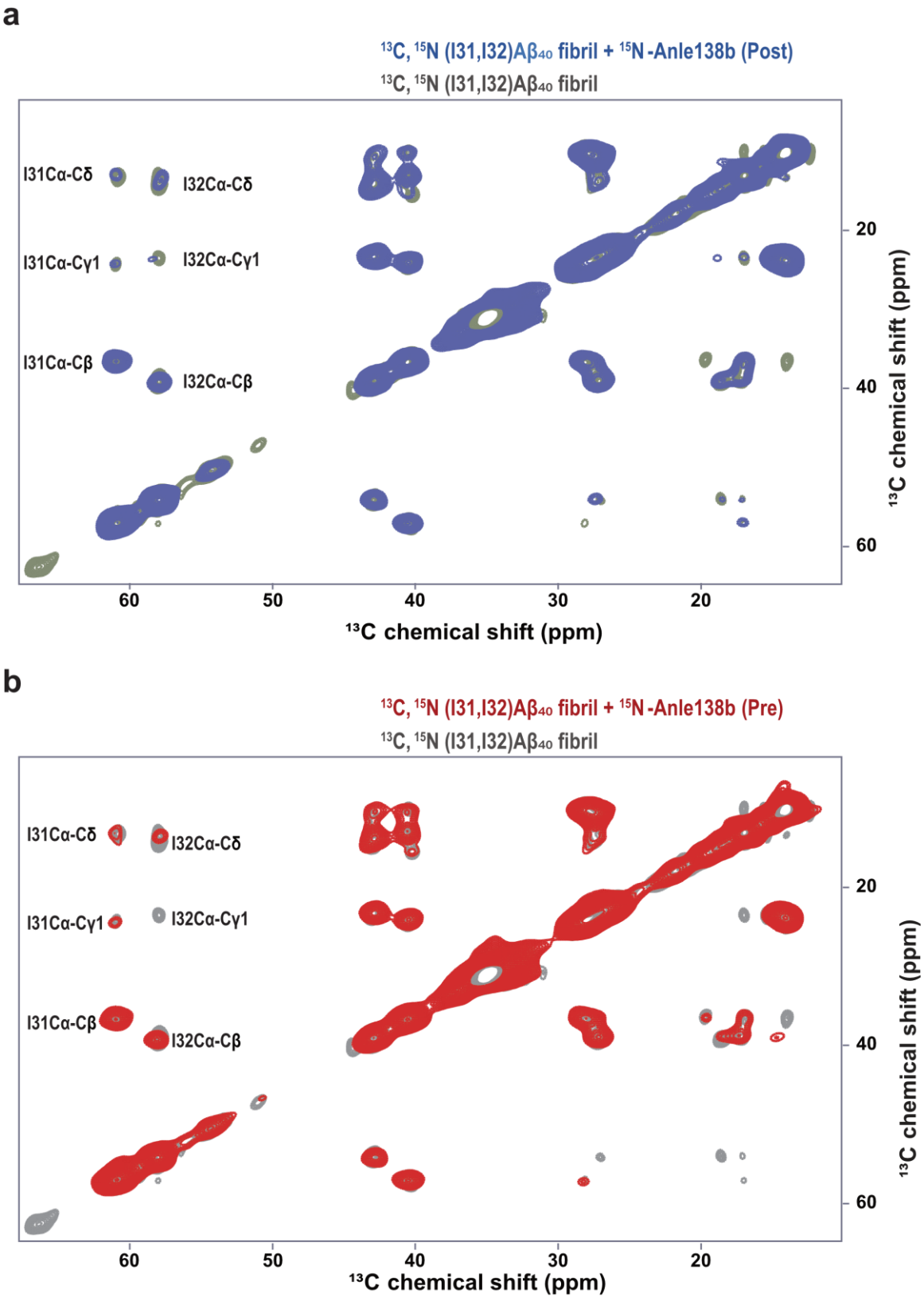
a
^{13}C, ^{15}N (I31,I32)Aβ$_{40}$ fibril + ^{15}N-Anle138b (Post)
^{13}C, ^{15}N (I31,I32)Aβ$_{40}$ fibril
I31Cα-Cδ
I32Cα-Cδ
I31Cα-Cγ1
I32Cα-Cγ1
I31Cα-Cβ
I32Cα-Cβ
60
50
40
30
20
^{13}C chemical shift (ppm)
20
40
60
^{13}C chemical shift (ppm)
b
^{13}C, ^{15}N (I31,I32)Aβ$_{40}$ fibril + ^{15}N-Anle138b (Pre)
^{13}C, ^{15}N (I31,I32)Aβ$_{40}$ fibril
I31Cα-Cδ
I32Cα-Cδ
I31Cα-Cγ1
I32Cα-Cγ1
I31Cα-Cβ
I32Cα-Cβ
60
50
40
30
20
^{13}C chemical shift (ppm)
20
40
60
^{13}C chemical shift (ppm)

Supplementary Figure 9 | 2D $^{13}C^{13}C$-DARR spectra of L1 $A\beta_{40}$ fibrils selectively labeled with ^{13}C, ^{15}N at Ile31 and Ile32.

a. 2D $^{13}C^{13}C$-DARR spectrum acquired at 265 K and 850 MHz with a mixing time of 20 ms. The blue spectrum corresponds to the post-treatment condition. **b.** The red spectrum represents the pre-treatment condition. In both panels, the gray spectrum represents the control condition.

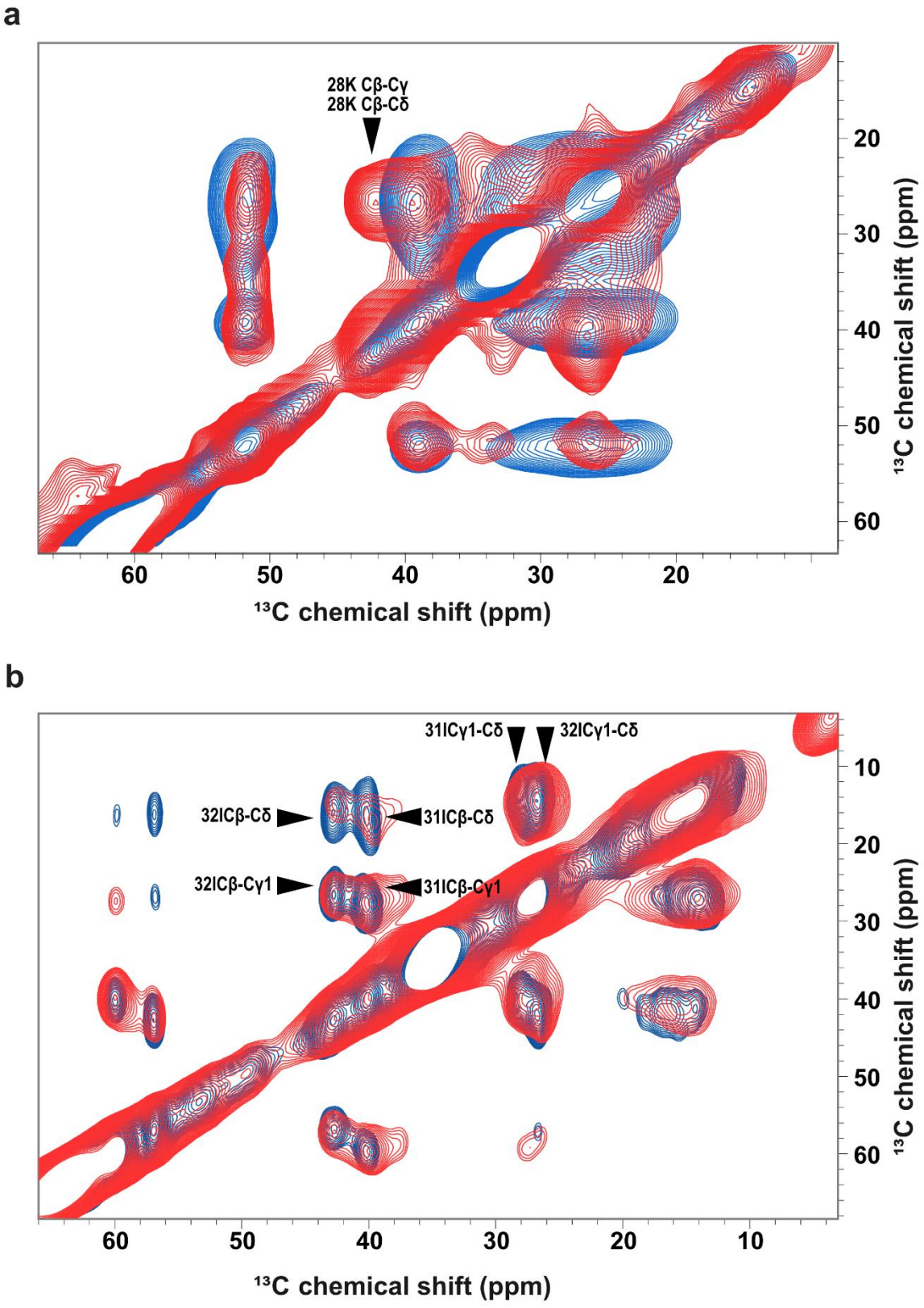
a
28K Cβ-Cγ
28K Cβ-Cδ
60
50
40
30
20
^{13}C chemical shift (ppm)
^{13}C chemical shift (ppm)
b
31ICγ1-Cδ
32ICγ1-Cδ
32ICβ-Cδ
31ICβ-Cδ
32ICβ-Cγ1
31ICβ-Cγ1
60
50
40
30
20
10
^{13}C chemical shift (ppm)
^{13}C chemical shift (ppm)

Supplementary Figure 10 | 2D $^{13}C^{13}C$- DARR and RFDR spectra of selectively labeled L1 $A\beta_{40}$ fibrils used for DNP experiments.

a. 2D $^{13}C^{13}C$–DARR spectra acquired at 100 K and 600 MHz with a mixing time of 50 ms under DNP conditions. Fibrils were selectively labeled with ^{13}C, ^{15}N at Lys16 and Lys28. The blue spectrum represents the post-treatment condition, in which anle138b was added after fibril formation. The red spectrum corresponds to the pre-treatment condition, where anle138b was present during fibril formation. **b.** 2D $^{13}C^{13}C$–RFDR spectra acquired under the same experimental conditions, with a mixing time of 2.6 ms. Fibrils were selectively labeled with ^{13}C, ^{15}N at Ile31 and Ile32. The blue spectrum corresponds to the post-treatment condition, and the red spectrum to the pre-treatment condition. Peak assignments include Cβ–Cγ and Cβ–Cδ correlations of Lys28 (**a**), and Cβ–Cγ1 and Cγ1–Cδ correlations of Ile31 and Ile32 (**b**). Arrows indicate assigned peaks.

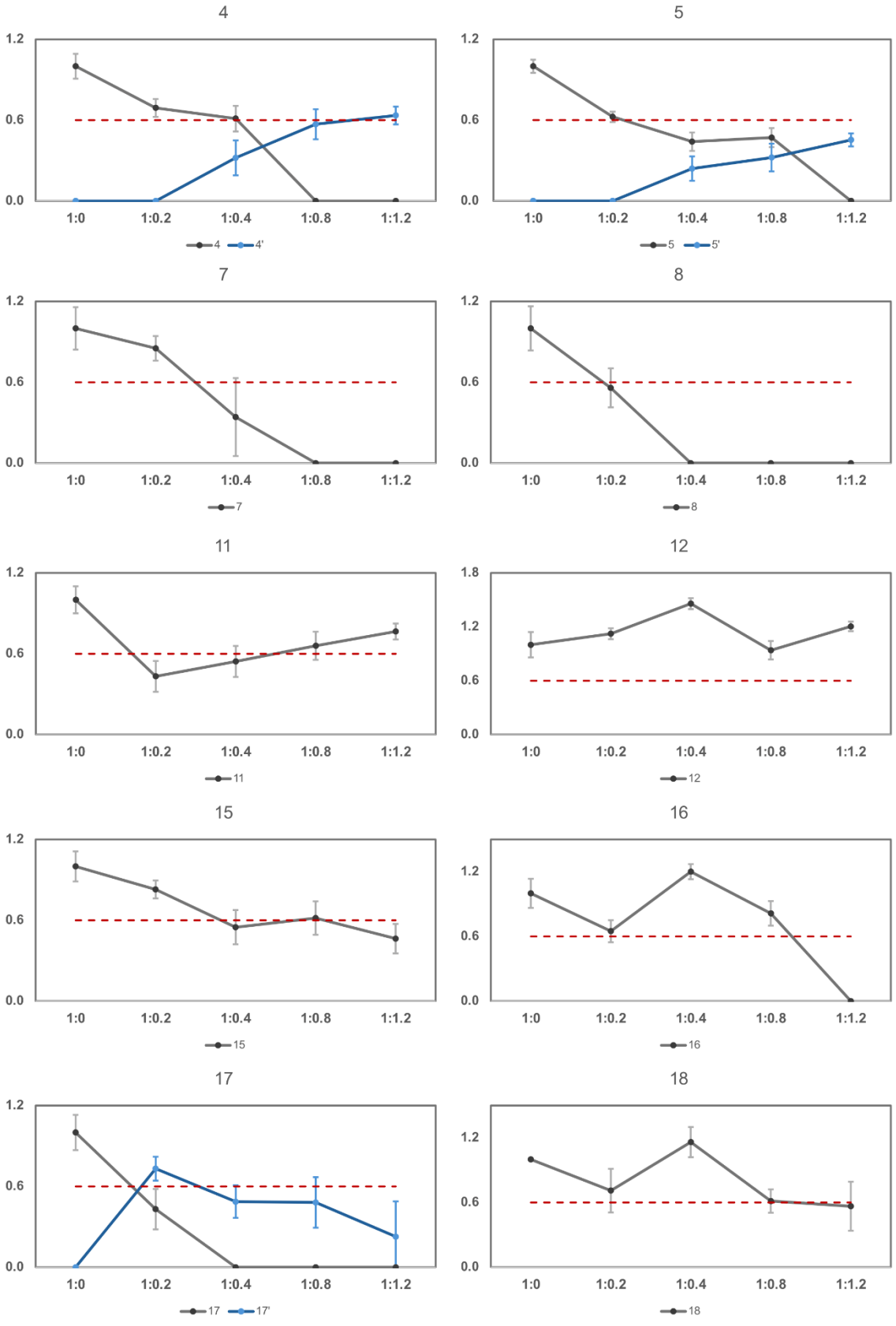
4
1.2
0.6
0.0
1:0
1:0.2
1:0.4
1:0.8
1:1.2
4
4'
5
1.2
0.6
0.0
1:0
1:0.2
1:0.4
1:0.8
1:1.2
5
5'
7
1.2
0.6
0.0
1:0
1:0.2
1:0.4
1:0.8
1:1.2
7
8
1.2
0.6
0.0
1:0
1:0.2
1:0.4
1:0.8
1:1.2
8
11
1.2
0.6
0.0
1:0
1:0.2
1:0.4
1:0.8
1:1.2
11
12
1.8
1.2
0.6
0.0
1:0
1:0.2
1:0.4
1:0.8
1:1.2
12
15
1.2
0.6
0.0
1:0
1:0.2
1:0.4
1:0.8
1:1.2
15
16
1.2
0.6
0.0
1:0
1:0.2
1:0.4
1:0.8
1:1.2
16
17
1.2
0.6
0.0
1:0
1:0.2
1:0.4
1:0.8
1:1.2
17
17'
18
1.2
0.6
0.0
1:0
1:0.2
1:0.4
1:0.8
1:1.2
18

Supplementary Figure 11 | Titration-dependent intensity changes indicating slow exchange binding of anle138b to residues 4–18 of L1 Aβ$_{40}$ fibrils.

Signal intensity ratios (I_ratio) were monitored for selected residues of L1 Aβ$_{40}$ as a function of increasing anle138b molar ratios (SMPR 1:0 to 1:1.2) under post-treatment conditions. The gray curves represent normalized intensities of original peaks (I_free) observed at SMPR 1:0, and their changes upon ligand titration (I_bound). The blue curves indicate new peaks indicative of slow exchange. The dashed red line marks the 0.6 intensity threshold used as a reference for qualitative comparison. I_ratio = I_bound / I_free, where I_free refers to the peak intensity in the absence of anle138b, and I_bound refers to the intensity at each titration point.

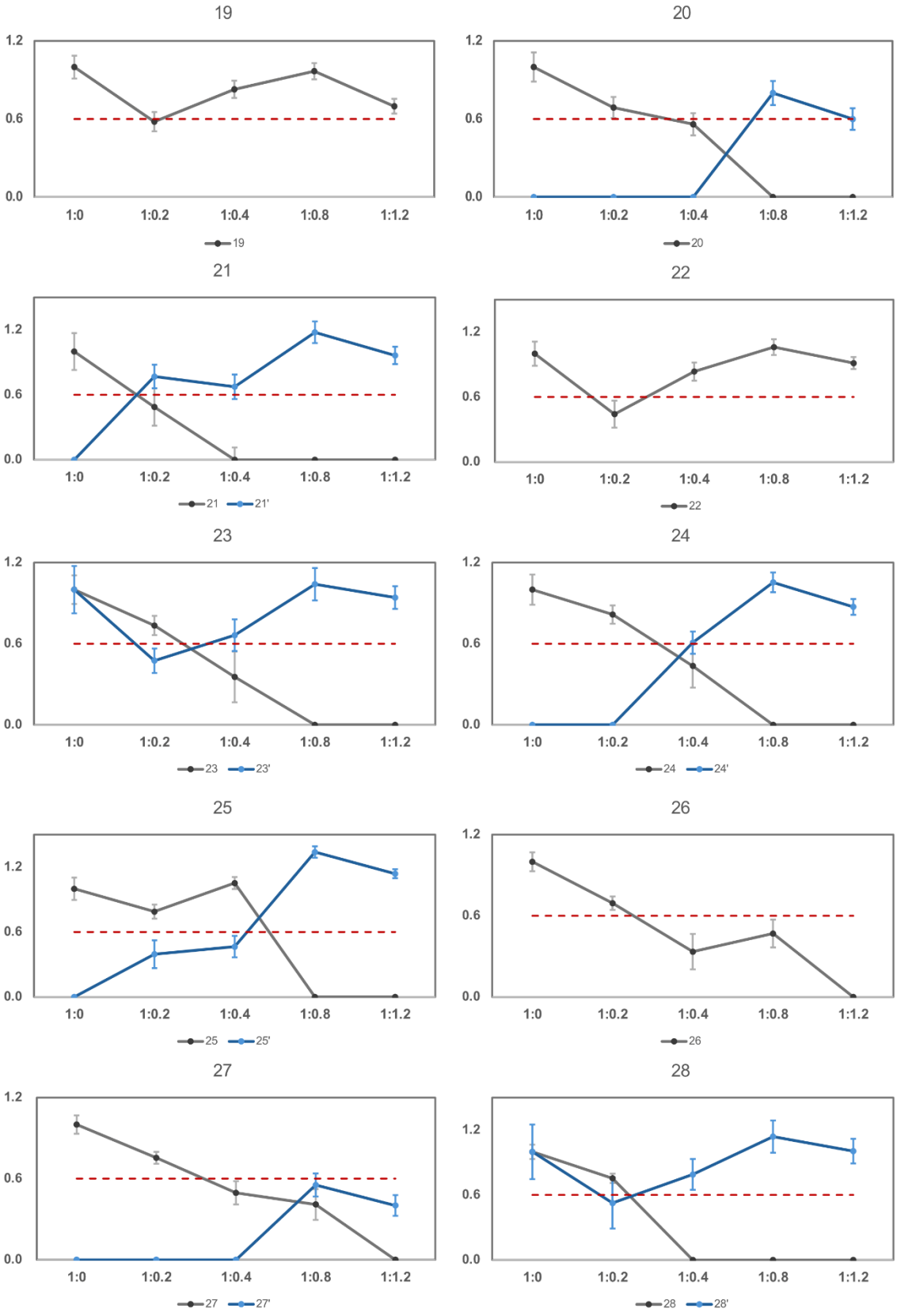
19
1.2
0.6
0.0
1:0
1:0.2
1:0.4
1:0.8
1:1.2
19
20
1.2
0.6
0.0
1:0
1:0.2
1:0.4
1:0.8
1:1.2
20
21
1.2
0.6
0.0
1:0
1:0.2
1:0.4
1:0.8
1:1.2
21
21'
22
1.2
0.6
0.0
1:0
1:0.2
1:0.4
1:0.8
1:1.2
22
23
1.2
0.6
0.0
1:0
1:0.2
1:0.4
1:0.8
1:1.2
23
23'
24
1.2
0.6
0.0
1:0
1:0.2
1:0.4
1:0.8
1:1.2
24
24'
25
1.2
0.6
0.0
1:0
1:0.2
1:0.4
1:0.8
1:1.2
25
25'
26
1.2
0.6
0.0
1:0
1:0.2
1:0.4
1:0.8
1:1.2
26
27
1.2
0.6
0.0
1:0
1:0.2
1:0.4
1:0.8
1:1.2
27
27'
28
1.2
0.6
0.0
1:0
1:0.2
1:0.4
1:0.8
1:1.2
28
28'

Supplementary Figure 12 | Titration-dependent intensity changes indicating slow exchange binding of anle138b to residues 19–28 of L1 $A\beta_{40}$ fibrils.

Signal intensity ratios (I_ratio) were monitored for selected residues of L1 $A\beta_{40}$ as a function of increasing anle138b molar ratios (SMPR 1:0 to 1:1.2) under post-treatment conditions. The gray curves represent normalized intensities of original peaks (I_free) observed at SMPR 1:0, and their changes upon ligand titration (I_bound). The blue curves indicate new peaks indicative of slow exchange. The dashed red line marks the 0.6 intensity threshold used as a reference for qualitative comparison. I_ratio = I_bound / I_free, where I_free refers to the peak intensity in the absence of anle138b, and I_bound refers to the intensity at each titration point.

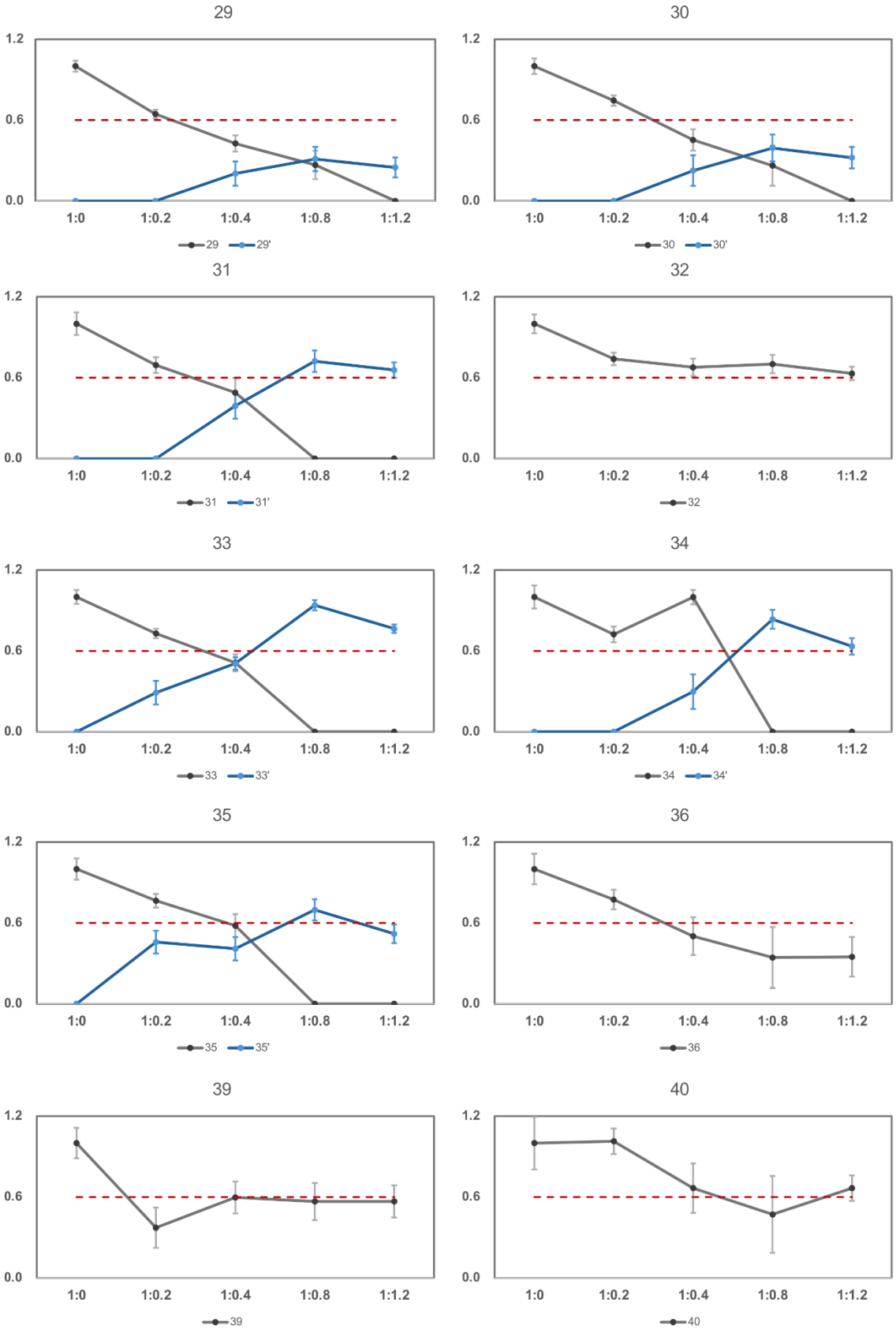
29
1.2
0.6
0.0
1:0
1:0.2
1:0.4
1:0.8
1:1.2
29
29'
30
30
30'
31
31
31'
32
32
33
33
33'
34
34
34'
35
35
35'
36
36
39
39
40
40

Supplementary Figure 13 | Titration-dependent intensity changes indicating slow exchange binding of anle138b to residues 29–40 of L1 $A\beta_{40}$ fibrils.

Signal intensity ratios (I_ratio) were monitored for selected residues of L1 $A\beta_{40}$ as a function of increasing anle138b molar ratios (SMPR 1:0 to 1:1.2) under post-treatment conditions. The gray curves represent normalized intensities of original peaks (I_free) observed at SMPR 1:0, and their changes upon ligand titration (I_bound). The blue curves indicate new peaks indicative of slow exchange. The dashed red line marks the 0.6 intensity threshold used as a reference for qualitative comparison. I_ratio = I_bound / I_free, where I_free refers to the peak intensity in the absence of anle138b, and I_bound refers to the intensity at each titration point.

a

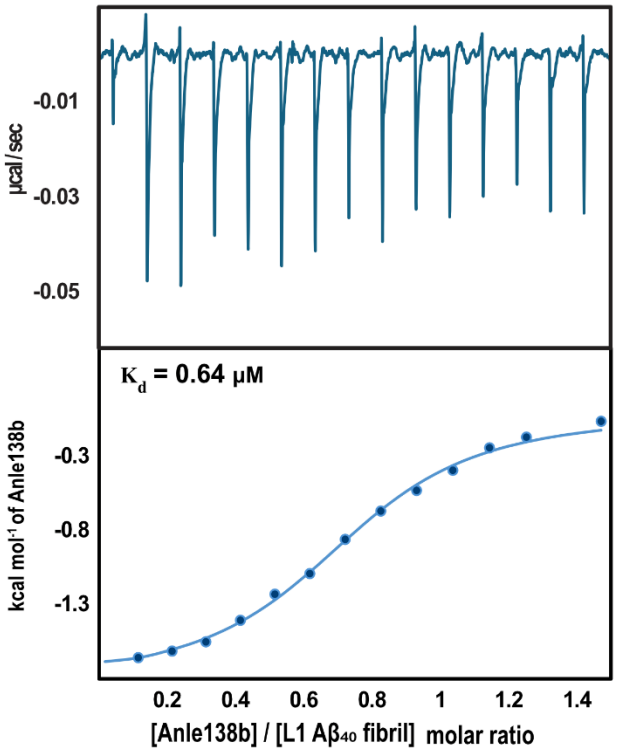
-0.01
-0.03
-0.05
µcal/sec
K_d = 0.64 µM
-0.3
-0.8
-1.3
kcal mol^{-1} of Anle138b
0.2
0.4
0.6
0.8
1
1.2
1.4
[Anle138b] / [L1 Aβ$_{40}$ fibril] molar ratio

b

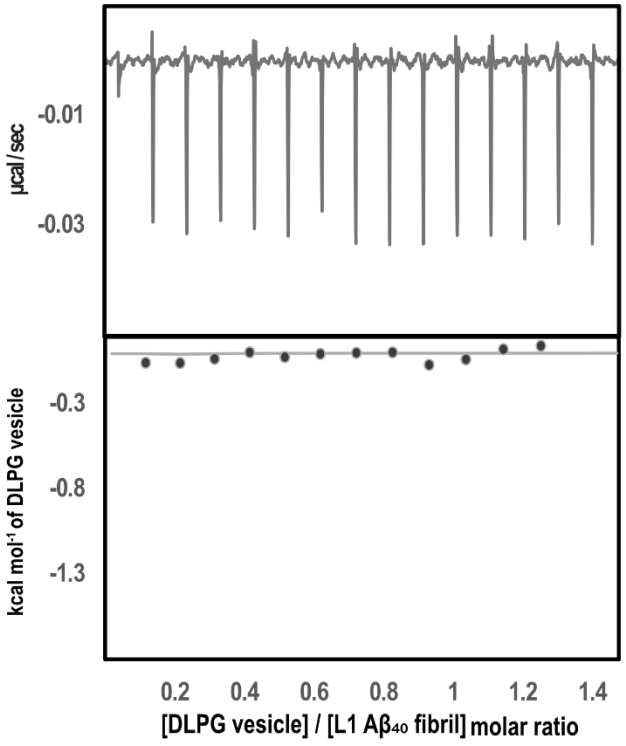
-0.01
-0.03
µcal/sec
-0.3
-0.8
-1.3
kcal mol^{-1} of DLPG vesicle
0.2
0.4
0.6
0.8
1
1.2
1.4
[DLPG vesicle] / [L1 Aβ$_{40}$ fibril] molar ratio

Supplementary Figure 14 | ITC analysis of anle138b and DLPG vesicle binding to L1 $A\beta_{40}$ fibrils.

The thermodynamic parameters for binding interaction are summarized in Tab. 2.

a. Isothermal titration calorimetry (ITC) thermogram (top) and integrated binding isotherm (bottom) of anle138b (100 µM), formulated in DLPG vesicles (2 mM), titrated into L1 $A\beta_{40}$ fibrils (10 µM). The fitted curve yields a dissociation constant (K_d) of 0.64 µM and a binding stoichiometry of ~0.72 anle138b molecules per $A\beta_{40}$ monomer. **b.** Negative control: Titration of DLPG vesicles (2 mM) into L1 $A\beta_{40}$ fibrils (10 µM) produces negligible heat and a flat isotherm, indicating no detectable interaction between vesicles and fibrils.

a

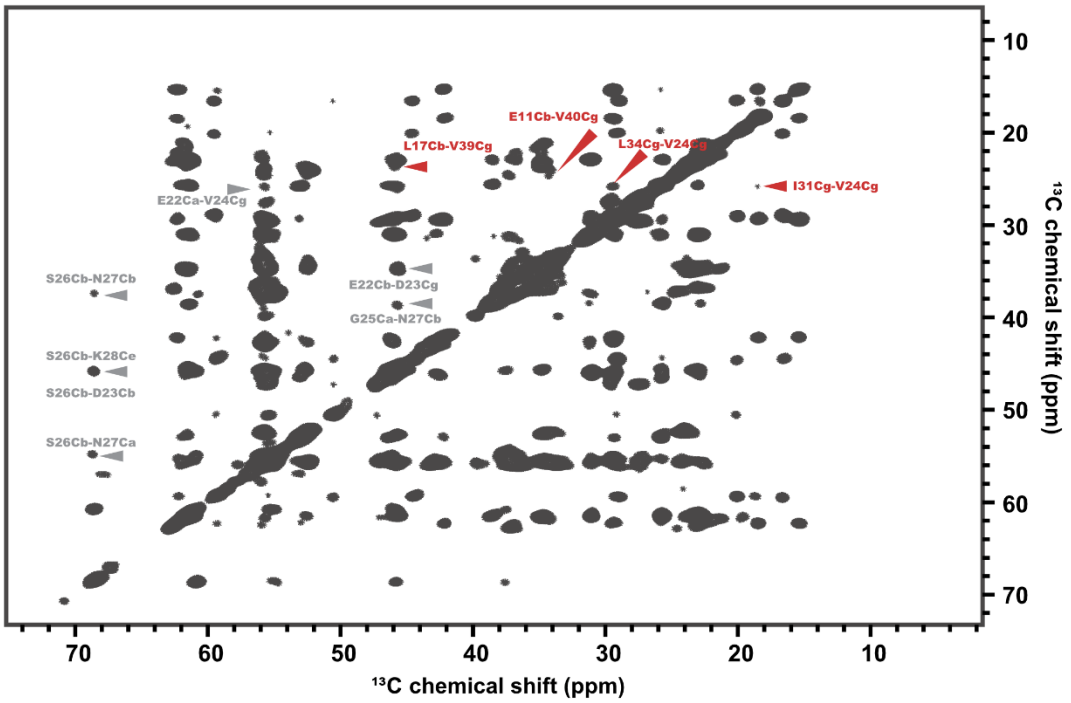
E11Cb-V40Cg
L17Cb-V39Cg
L34Cg-V24Cg
I31Cg-V24Cg
E22Ca-V24Cg
E22Cb-D23Cg
G25Ca-N27Cb
S26Cb-N27Cb
S26Cb-K28Ce
S26Cb-D23Cb
S26Cb-N27Ca
70
60
50
40
30
20
10
^{13}C chemical shift (ppm)
^{13}C chemical shift (ppm)

b

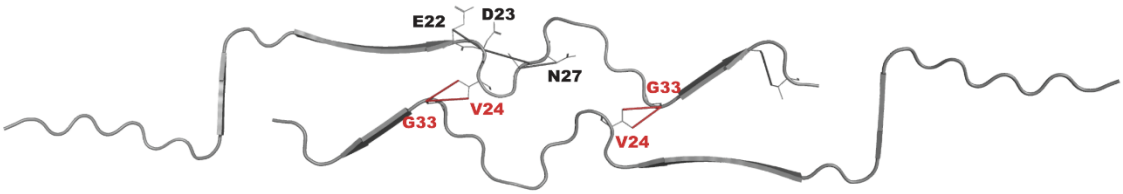
E22
D23
N27
G33
V24
G33
V24

c

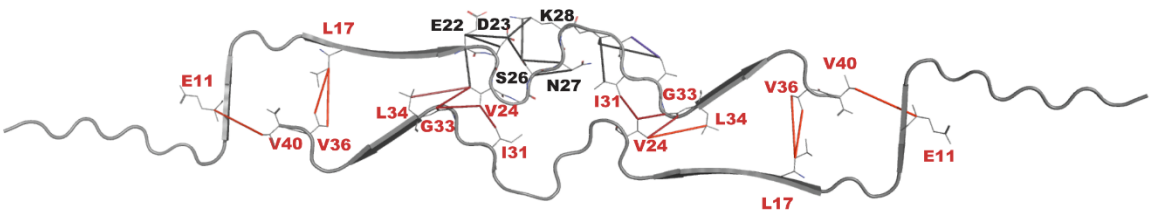
L17
E22
D23
K28
E11
S26
N27
I31
G33
V40
L34
V24
V36
L34
G33
V40
V36
I31
V24
E11
L17

Supplementary Figure 15 | 2D $^{13}C^{13}C$-DARR spectrum (265K, 850MHz) of L1 Aβ$_{40}$ fibrils.

a. Aliphatic region of the 2D ^{13}C–^{13}C chemical shift correlation spectrum acquired at 265 K and 850 MHz (mixing time =200 ms). Gray arrows indicate medium-range intramolecular cross-peaks (2–4 Å); red arrows indicate medium-to-long-range intermolecular cross-peaks (3–5 Å). **b.** The structural model of L1 Aβ$_{40}$ fibrils shows the intramolecular contacts (gray bars, mixing time = 50 ms). **c.** The same structural model highlights the intra- and intermolecular contacts (gray and red bars, respectively, mixing time = 200 ms).

a

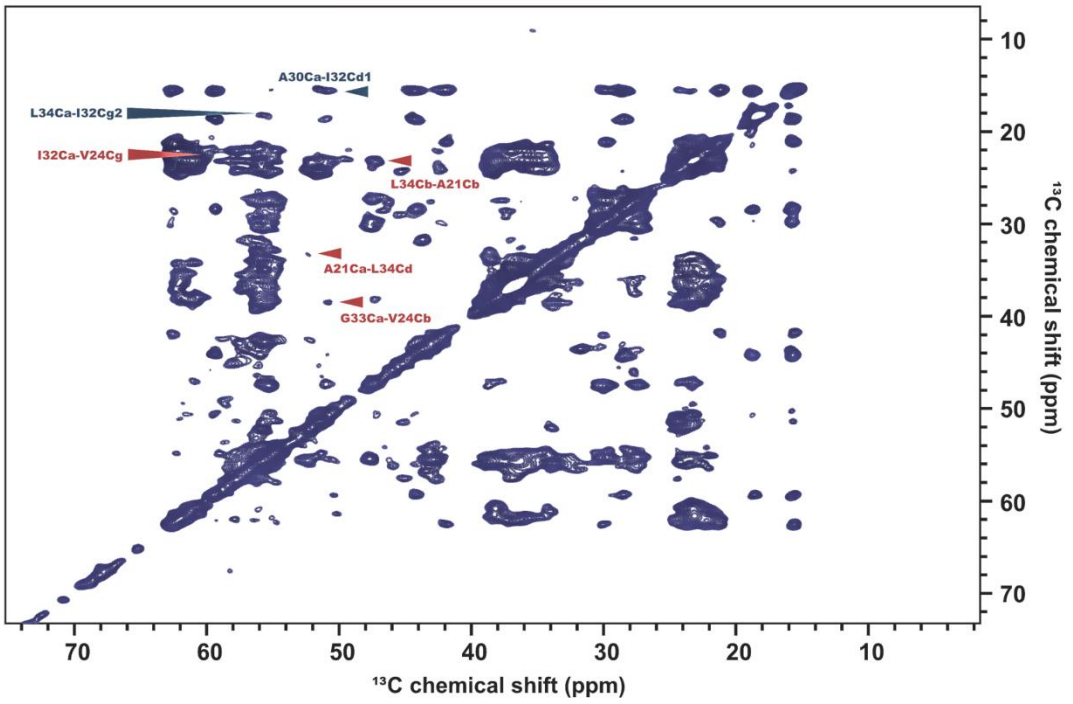
A30Ca-I32Cd1
L34Ca-I32Cg2
I32Ca-V24Cg
L34Cb-A21Cb
A21Ca-L34Cd
G33Ca-V24Cb
10
20
30
40
50
60
70
70
60
50
40
30
20
10
^{13}C chemical shift (ppm)
^{13}C chemical shift (ppm)

b

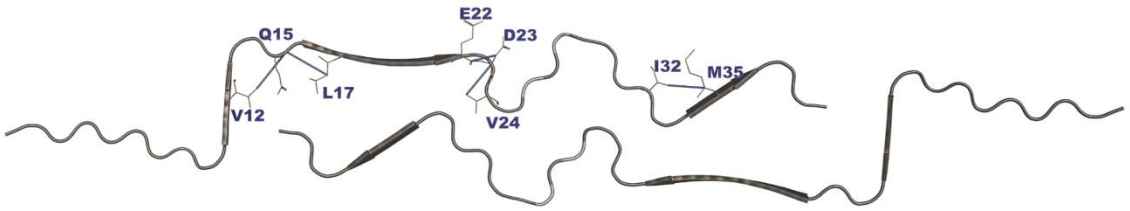
E22
Q15
D23
I32
M35
L17
V12
V24

c

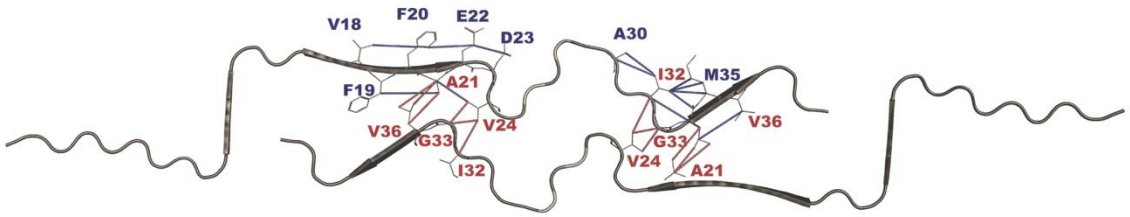
V18
F20
E22
D23
A30
I32
M35
F19
A21
V36
V24
G33
I32
V36
G33
V24
A21

Supplementary Figure 16 | 2D $^{13}C^{13}C$-DARR spectrum (265K, 850MHz) of L1 Aβ$_{40}$ fibrils (post-treatment condition).

Anle138b was applied to L1 Aβ$_{40}$ fibrils after fibril formation (Aβ$_{40}$: anle138b (SMPR) = 1: 1.2). **a.** Aliphatic region of the 2D ^{13}C–^{13}C chemical shift correlation spectrum acquired at 265 K and 850 MHz (mixing time =200 ms). Blue arrows indicate medium-range intramolecular cross-peaks (2–4 Å); red arrows indicate medium-to-long-range intermolecular cross-peaks (3–5 Å). **b.** The structural model of L1 Aβ$_{40}$ fibrils shows the intramolecular contacts (blue bars, mixing time = 50 ms). **c.** The same structural model highlights the intra- and intermolecular contacts (blue and red bars, respectively, mixing time = 200 ms).

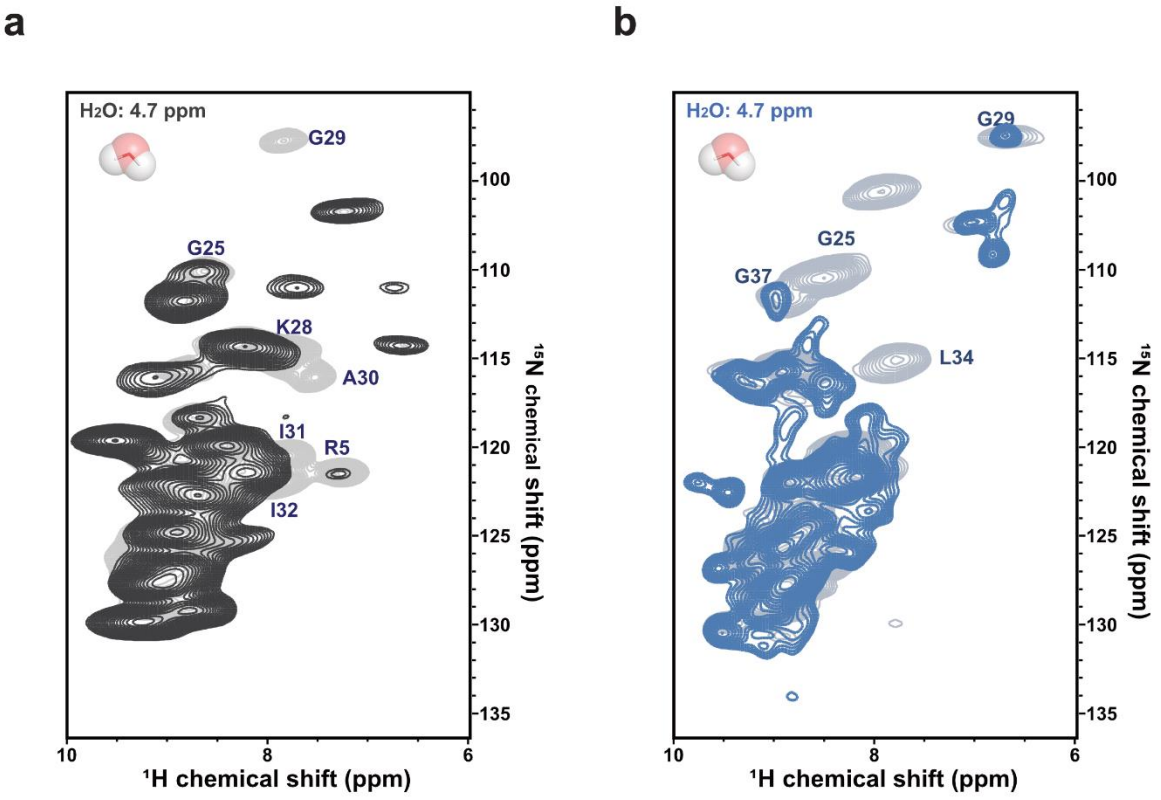
a
H2O: 4.7 ppm
G29
G25
K28
A30
I31
R5
I32
15N chemical shift (ppm)
1H chemical shift (ppm)
b
H2O: 4.7 ppm
G29
G25
G37
L34
15N chemical shift (ppm)
1H chemical shift (ppm)

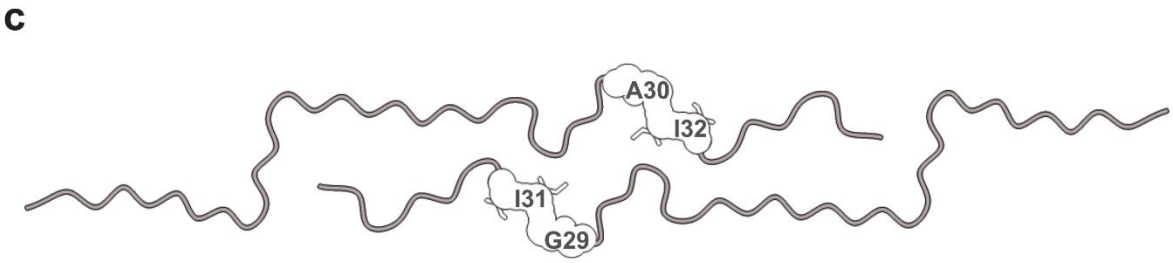
c
A30
I32
I31
G29


d
G25
L34

Supplementary Figure 17 | Comparison of H_2O-accessible amide groups in L1 $A\beta_{40}$ fibrils under control and post-treatment conditions.

a. Light gray: 2D (H)NH spectrum of ^{2}H, ^{13}C, ^{15}N-labeled L1 $A\beta_{40}$ fibrils (control). Dark gray: 2D plane at 4.7 ppm (water signal) in the H dimension was extracted from a 3D H(H)NH NOE spectrum with a 50 ms mixing time. Cross-peaks in dark gray indicate amide groups in close contact with H_2O under control conditions. **b.** Light gray: 2D (H)NH spectrum of ^{2}H, ^{13}C, ^{15}N-labeled L1 $A\beta_{40}$ fibrils under post-treatment conditions. Blue: 2D slice from a 3D H(H)NH NOE spectrum (50 ms mixing) at 4.7 ppm. Blue cross-peaks indicate water-accessible amides in the post-treatment condition. **c.** Structural map of control fibrils, with gray-colored residues indicating H_2O-accessible amides. **d.** Structural map of post-treatment fibrils, with blue-colored residues indicating water-accessible amides. Residues with no detectable water contact are shown as white spheres.

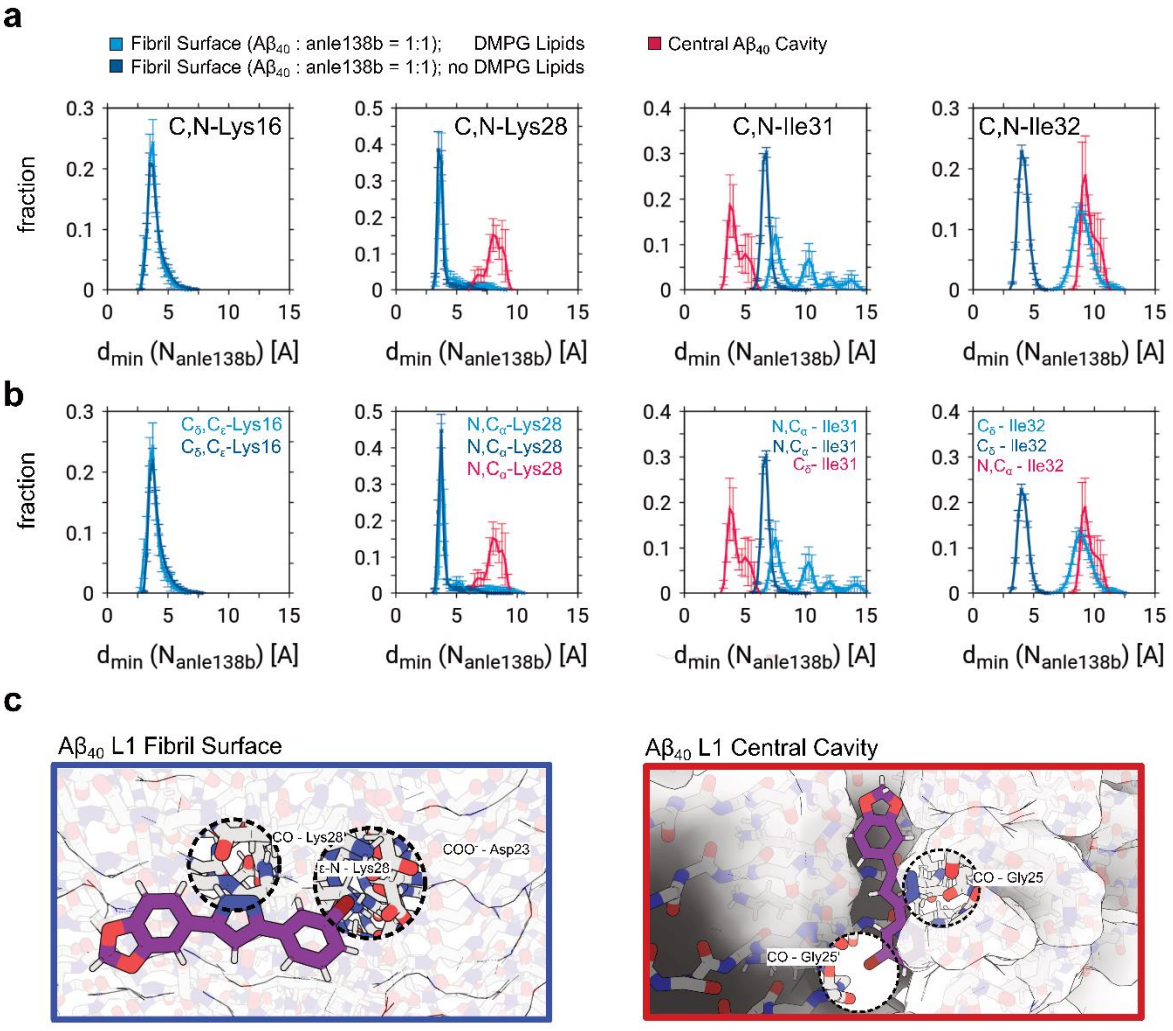
a
Fibril Surface (Aβ40 : anle138b = 1:1); DMPG Lipids
Fibril Surface (Aβ40 : anle138b = 1:1); no DMPG Lipids
Central Aβ40 Cavity
C,N-Lys16
C,N-Lys28
C,N-Ile31
C,N-Ile32
fraction
dmin (Nanle138b) [A]
b
Cδ,Cε-Lys16
Cδ,Cε-Lys16
N,Cα-Lys28
N,Cα-Lys28
N,Cα-Lys28
N,Cα - Ile31
N,Cα - Ile31
Cδ- Ile31
Cδ - Ile32
Cδ - Ile32
N,Cα - Ile32
c
Aβ40 L1 Fibril Surface
CO - Lys28
ε-N - Lys28
COO- - Asp23
Aβ40 L1 Central Cavity
CO - Gly25
CO - Gly25

Supplementary Figure 18 | Dominant binding poses and interatomic contacts of surface-bound and internally bound anle138b.

a. Distributions of minimum distances derived from all N or C atoms of residues K16, K28, I31, and I32 to anle138b pyrazole nitrogen atoms for the simulation sets representing either surface-bound (blue and dark blue: without DMPG) or internally bound (red) anle138b. **b.** Distributions of minimum distances derived from the individual N and/or C atoms of residues K16, K28, I31, and I32 to anle138b pyrazole nitrogen atoms that best fit the distributions in **a** and **c.** Representative MD simulation snapshot of anle138b binding poses and interatomic contacts as observed for L1 $A\beta_{40}$ surface-bound (left panel) or internally bound (right panel). Circles highlight interatomic contacts: Lys28 carbonyl to anle138b pyrazole and Asp23/Lys28 side chain to anle138b bromophenyl interaction (left), as well as Gly25 carbonyl to anle138b pyrazole and Gly25 carbonyl (opposing protofilament) to anle138b bromophenyl interaction (right). DMPG lipids are not shown for clarity.

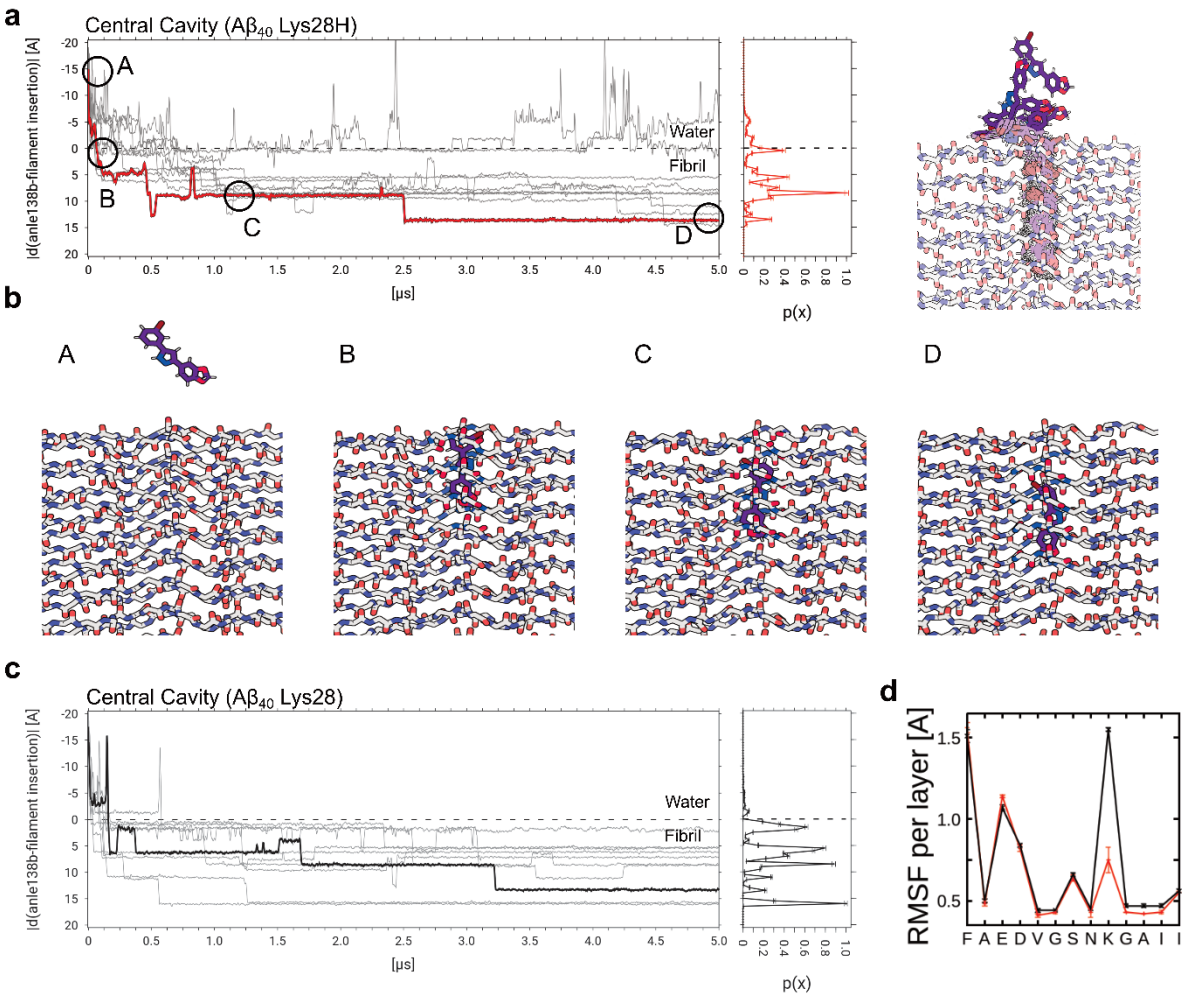
a
Central Cavity (Aβ40 Lys28H)
|d(anle138b-filament insertion)| [A]
A
B
C
D
Water
Fibril
[μs]
p(x)
b
A
B
C
D
c
Central Cavity (Aβ40 Lys28)
|d(anle138b-filament insertion)| [A]
Water
Fibril
[μs]
p(x)
d
RMSF per layer [A]
F A E D V G S N K G A I I

Supplementary Figure 19 | Anle138b inserts spontaneously in the central cavity of $A\beta_{40}$ L1 fibrils.

a. Distance of the anle138b pyrazole nitrogen atoms to the fibril center-of-mass (representative trajectory as bold lines: color red; others as shaded thin lines for clarity: color gray) and **b.** snapshots (A, B, C, D) from MD simulations of anle138b spontaneously binding internally to the cavity of L1, as well as it's discrete translational motion along the fibril axis. **c.** Distance of the anle138b pyrazole nitrogen atoms to the fibril center-of-mass for simulations with deprotonated Lys28 i.e. disrupted hydrogen bond interaction between Asp23 and Lys28. The **histograms** (panels on the right) in **a** and **c** were calculated over the full trajectory length, respectively. Simulations in **a** show that deeper or comparable insertion to **c** does not occur on the multi μs-time scales accessible by the reported MD simulations. **d.** Average root mean squared fluctuations (RMSF) for residues of the loop region with (red) and without (black) intact Asp23-Lys28 hydrogen bond. Data are presented as mean values ± SEM (depicted by error bars).

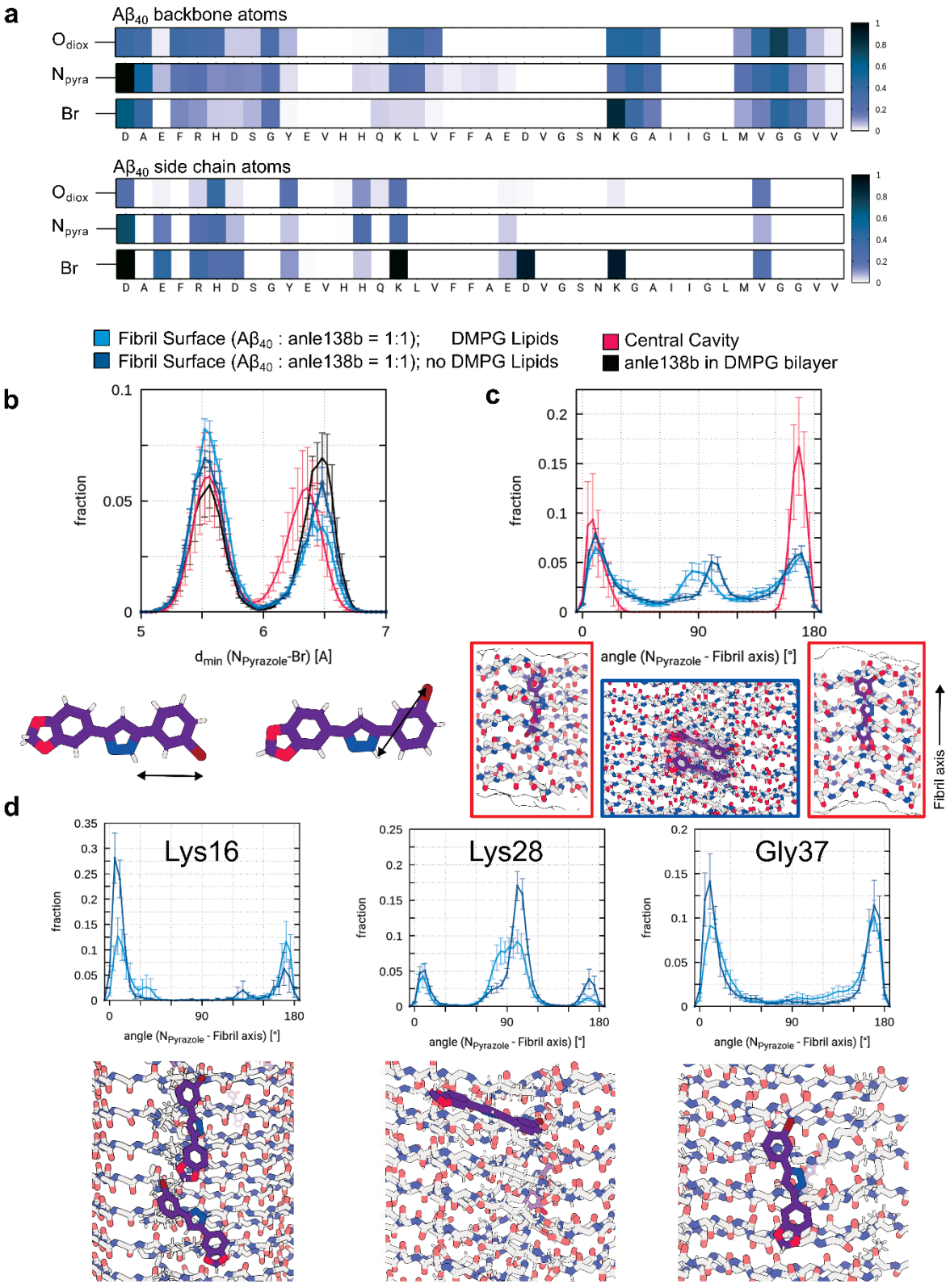
a
Aβ40 backbone atoms
Odiox
Npyra
Br
D A E F R H D S G Y E V H H Q K L V F F A E D V G S N K G A I I G L M V G G V V
Aβ40 side chain atoms
Fibril Surface (Aβ40 : anle138b = 1:1); DMPG Lipids
Fibril Surface (Aβ40 : anle138b = 1:1); no DMPG Lipids
Central Cavity
anle138b in DMPG bilayer
b
fraction
dmin (NPyrazole-Br) [A]
c
angle (NPyrazole - Fibril axis) [°]
Fibril axis
d
Lys16
Lys28
Gly37

Supplementary Figure 20 | Anle138b binding modes to the surface and central cavity of L1 Aβ$_{40}$ fibrils.

a. Heat maps report polar contacts between backbone and side chain atoms of individual L1 Aβ$_{40}$ fibril structure residues and polar moieties of anle138b, respectively. Scale bars indicate contact probabilities. **b.** Distance distribution of anle138b pyrazole N to Bromine atom (blue – surface-bound anle138b; red - internal binding pose, black – anle138b in DMPG bilayer). **c.** Anle138b alignment with respect to the fibril axis when bound either internally to the loop region (red) or to the surface of the L1 Aβ$_{40}$ fibrils (blue). **d.** Anle138b alignment with respect to the fibril axis when bound to residues Lys16, Lys28, and Gly37 of the L1 Aβ$_{40}$ fibril surface. Representative snapshots of anle138b binding poses are shown. DMPG lipids are not depicted for clarity.

Supplementary Table 1 | Experimental parameters of NMR data acquisition on the sample.

Exp	Spectrometer	MAS (kHz) rotor	Transfer	Nucleus	time cp (ms)	rf (kHz)	Ramp	Temperature	Sample
3D (H)CANH	800, Advance III	55 (1.3mm)	^{1}H-^{13}C-CP	^{1}H	6.5	96	80-100%	235K	^{2}H,^{13}C,^{15}N Aβ$_{40}$ fibril ^{2}H,^{13}C,^{15}N Aβ$_{40}$ fibril: Anle138b = 1:0.2, 1: 0.4, 1:0.8, 1:1.2 (titration)
				^{13}C		88	square		
			^{13}C-^{15}N-CP	^{13}C	20	139.1	tangent		
				^{15}N		57	square		
			^{15}N-^{1}H-CP	^{1}H		145	100-80%		
				^{15}N	0.7	85			
3D (H)coCAcoNH	800, Advance III	55 (1.3mm)	^{1}H-^{13}C-CP	^{1}H	2.9	22	85-100%	235K	^{2}H,^{13}C,^{15}N Aβ$_{40}$ fibril: Anle138b = 1:1.2
				^{13}C		17	square		
			^{13}C-^{15}N-CP	^{13}C	25	17	tangent		
				^{15}N		15	square		
			^{15}N-^{1}H-CP	^{1}H	8	24	100-80%		
				^{15}N	0.85	20.7			
2D (H)NH	800, Advance III	55 (1.3mm)	^{15}N-^{1}H-CP	^{1}H	3.1	97	100-80%	235K	^{2}H,^{13}C,^{15}N Aβ$_{40}$ fibril: Anle138b = 1:1.2
				^{15}N		170			
			^{1}H-^{15}N-CP	^{1}H	0.9	104	80-100%		
				^{15}N		170			
3D H(H)NH NOE	800, Advance III	55 (1.3mm)	^{15}N-^{1}H-CP	^{1}H	3.1	90	100-80%	235K	^{2}H,^{13}C,^{15}N Aβ$_{40}$ fibril: Anle138b = 1:1.2
				^{15}N		152			
			^{1}H-^{15}N-CP	^{1}H	0.9	99	80-100%		

				^{15}N		166			
2D ^{13}C-^{13}C-DARR (20ms, 50ms, 200ms, 400ms)	850, NEO	17 (3.2mm)	^{1}H-^{13}C-CP	^{1}H		80	100-80%	265K	^{1}H,^{13}C,^{15}N Aβ$_{40}$ fibril ^{1}H,^{13}C,^{15}N Aβ$_{40}$ fibril: Anle138b = 1:1.2 (Post-treatment condition) ^{1}H,^{13}C,^{15}N Aβ$_{40}$ fibril: Anle138b = 1:1.2 (Pre-treatment condition)
				^{13}C	1.1	88			
3D (H)CANH	850, NEO	55 (1.3mm)	^{1}H-^{13}C-CP	^{1}H	2.9	22	85-100%	235K	^{1}H,^{13}C,^{15}N Aβ$_{40}$ fibril
				^{13}C		17	square		
			^{13}C-^{15}N-CP	^{13}C	25	17	tangent		
				^{15}N		15	square		
			^{15}N-^{1}H-CP	^{1}H		24	100-80%		
				^{15}N	0.8	20.7			
2D (H)NCA	850, NEO	17 (3.2mm)	^{13}C-^{15}N-CP	^{13}C	3	16	100-90%	265K	^{1}H,^{13}C,^{15}N Aβ$_{40}$ fibril ^{1}H,^{13}C,^{15}N Aβ$_{40}$ fibril: Anle138b = 1:1.2 (Pre-treatment condition) ^{1}H,^{13}C,^{15}N Aβ$_{40}$ fibril: Anle138b = 1:1.2 (Pre-treatment condition)
				^{15}N		18			
			^{1}H-^{15}N-CP	^{1}H	1.5	83	80-100%		
				^{15}N		73			

2D ^{13}C-^{13}C-DARR (20ms)	850, NEO	17 (3.2mm)	^{1}H-^{13}C-CP	^{1}H		80	100-80%	265K	ILE ^{13}C,^{15}N Aβ40 fibril ILE ^{13}C,^{15}N Aβ40 fibril: Anle138b = 1:1.2 (Post-treatment condition)
				^{13}C	1.5	88			ILE ^{13}C,^{15}N Aβ40 fibril: Anle138b = 1:1.2 (Pre-treatment condition)
2D ^{13}C-^{13}C-DARR (20ms)	850, NEO	17 (3.2mm)	^{1}H-^{13}C-CP	^{1}H		80	100-80%	265K	LYS ^{13}C,^{15}N Aβ40 fibril LYS ^{13}C,^{15}N Aβ40 fibril: Anle138b = 1:1.2 (Post -fibril condition)
				^{13}C	1.2	88			LYS ^{13}C,^{15}N Aβ40 fibril: Anle138b = 1:1.2 (Pre-treatment condition)
2D ^{13}C-^{13}C-RFDR (2.6ms)	600, Advance III e = 6 ~8 TEMTRIPol-1	10 (3.2mm)	^{1}H-^{13}C-CP	^{1}H		98	90-100%	100K (DNP)	ILE ^{13}C,^{15}N Aβ40 fibril: Anle138b = 1:1.2 (Post-treatment condition)
				^{13}C	0.9	77			ILE ^{13}C,^{15}N Aβ40 fibril: Anle138b = 1:1.2 (Pre-treatment condition)
2D ^{13}C-^{13}C-DARR (50ms)	600, Advance III e = 6 ~8 TEMTRIPol-1	10 (3.2mm)	^{1}H-^{13}C-CP	^{1}H		70.8	90-100%	100K (DNP)	LYS ^{13}C,^{15}N Aβ40 fibril: Anle138b = 1:1.2 (Post-treatment condition)

				^{13}C	0.6				LYS ^{13}C,^{15}N Aβ$_{40}$ fibril: Anle138b = 1:1.2 (Pre-treatment condition)
2D NHHC	600, Advance III e = 6 ~8 TEMTRIPol-1	10 (3.2mm)	^{1}H-^{15}N-CP	^{1}H	0.35	49	90-100%	100K (DNP)	^{1}H,^{13}C,^{15}N Aβ$_{40}$ fibril: Anle138b = 1:1.2 (Pre-treatment condition)
				^{15}N		32			
			^{15}N-^{1}H--CP	^{15}N		32			^{1}H,^{13}C,^{15}N Aβ$_{40}$ fibril: Anle138b = 1:1.2 (Pre-treatment condition)
				^{1}H	0.35	49	80-100%		
			^{1}H-^{13}C-CP	^{1}H		61	80-100%		
				^{13}C	0.6	84			
2D NHHC	600, Advance III e = 6 ~8 TEMTRIPol-1	10 (3.2mm)	^{1}H-^{15}N-CP	^{1}H	0.36	39	90-100%	100K (DNP)	LYS ^{13}C,^{15}N Aβ$_{40}$ fibril: Anle138b = 1:1.2 (Post-treatment condition)
				^{15}N		31			
			^{15}N-^{1}H--CP	^{15}N		31			LYS ^{13}C,^{15}N Aβ$_{40}$ fibril: Anle138b = 1:1.2 (Pre-treatment condition)
				^{1}H	0.6	39	80-100%		
			^{1}H-^{13}C-CP	^{1}H		67	80-100%		
				^{13}C	0.7	61			
2D NHHC	600, Advance III e = 6 ~8 TEMTRIPol-1	10 (3.2mm)	^{1}H-^{15}N-CP	^{1}H	0.5	43	90-100%	100K (DNP)	ILE ^{13}C,^{15}N Aβ$_{40}$ fibril: Anle138b = 1:1.2 (Post-treatment condition)
				^{15}N		33			
			^{15}N-^{1}H--CP	^{15}N		33			ILE ^{13}C,^{15}N Aβ$_{40}$ fibril: Anle138b = 1:1.2 (Pre-treatment fibril condition)
				^{1}H	0.3	43	80-100%		
			^{1}H-^{13}C-CP	^{1}H		98	80-100%		
				^{13}C	0.7	77			

Supplementary Table 2 | Thermodynamic parameters obtained from ITC titrations of anle138b (in DLPG vesicle) or DLPG vesicle alone into L1 $A\beta_{40}$ fibrils.

Control titration results using DLPG vesicles without anle138b are shown in Supplementary Fig. 14 b, while titrations with DLPG vesicles containing anle138b are shown in Fig. 4 b and Supplementary Fig. 14a.

	[Anle138b (DLPG vesicle)] / [L1 $A\beta_{40}$ fibril]	**[DLPG vesicle] / [L1 $A\beta_{40}$ fibril]**
[Cell] (µM)	10.00	10.00
[Syringe] (µM)	100.00	100.00
N (sites)	0.72 ± 0.01	
KD (µM)	0.64 ± 0.068	
ΔH (kcal/mol)	-1.84 ± 0.039	
ΔG (kcal/mol)	-8.45	
-TΔS (kcal/mol)	-6.62	

Supplementary Table 3 | Cryo-EM structure determination statistics.

	Post-treatment $A\beta_{40}$ fibril	Pre-treatment $A\beta_{40}$ fibril
Data collection		
Microscope	Titan Krios G2	Titan Krios G2
Voltage [keV]	300	300
Detector	K3	K3
Magnification	81,000	81,000
Pixel size [Å]	1.05	1.05
Defocus range [μm]	-0.7 to -2.4	-0.7 to -2.4
Exposure time [s/frame]	3.0	2.95
Number of frames	40	40
Total dose [$e^-/Å^2$]	~40	~40
	(~1.0 $e^-/Å^2$/frame)	(~1.0 $e^-/Å^2$/frame)
Reconstruction		
Micrographs	7,311	21,576
Box width [pixels]	250	250
Inter-box distance [pixels]	13	13
Picked segments (no.)	3,193,361	9,147,664
Final map[a]		
Final segments [no.]	326,836	888,252
Final resolution [Å] (FSC=0.143)	2.79	2.76
Applied map sharpening B-factor [$Å^2$]	-114	-121
Symmetry imposed	C1	C1
Helical rise [Å]	2.35	2.35
Helical twist [°]	179.65	179.65

[a] Sharpened map and refined atomic model are provided as SI files.

Supplementary Table 4 | Model building statistics.

Lipid-induced PM	Post-treatment $A\beta_{40}$ fibril	Pre-treatment $A\beta_{40}$ fibril
Initial model [PDB code]	8ovk	8ovk
Model composition[a]		
Chains	10	10
Non-hydrogen atoms	3060	3060
Protein residues	400	400
RMS deviations		
Bond lengths [Å]	0.02	0.01
Bond angles [°]	2.23	2.09
Validation		
MolProbity score	1.68	1.70
Clashscore	5.86	6.19
Ramachandran plot		
Outliers [%]	0	0
Allowed [%]	5.26	5.26
Favored [%]	94.74	94.74

[a] Sharpened map and refined atomic model l.